UHASSELT
KNOWLEDGE IN ACTION

Maastricht University

Faculty of Medicine and Life Sciences
School for Life Sciences
Master of Biomedical Sciences

Master's thesis

Nanoparticle-specific effects on the differentiation capacity and mitochondrial function of human dental pulp stem cells

Ellen Browko

Thesis presented in fulfillment of the requirements for the degree of Master of Biomedical Sciences, specialization Environmental Health Sciences

SUPERVISOR :

dr. Nelly SAENEN

Prof. dr. Karen SMEETS

MENTOR :

Mevrouw Margo WITTERS

2021
2022

Transnational University Limburg is a unique collaboration of two universities in two countries: the University of Hasselt and Maastricht University.

UHASSELT
KNOWLEDGE IN ACTION

www.uhasselt.be
Universiteit Hasselt
Campus Hasselt:
Martelarenlaan 42 | 3500 Hasselt
Campus Diepenbeek:
Agoralaan Gebouw D | 3590 Diepenbeek

UHASSELT
KNOWLEDGE IN ACTION

Maastricht University

Faculty of Medicine and Life Sciences
School for Life Sciences
Master of Biomedical Sciences

Master's thesis

Nanoparticle-specific effects on the differentiation capacity and mitochondrial function of human dental pulp stem cells

Ellen Browko

Thesis presented in fulfillment of the requirements for the degree of Master of Biomedical Sciences, specialization Environmental Health Sciences

SUPERVISOR :

dr. Nelly SAENEN

Prof. dr. Karen SMEETS

MENTOR :

Mevrouw Margo WITTERS

Nanoparticle-specific effects on the differentiation capacity and mitochondrial function of human dental pulp stem cells *

Browko Ellen[1], Witters Margo1[1], Jaenen Vincent[1], Saenen Nelly[1] and Smeets Karen[1]

[1]Zoology research group, Biodiversity and Toxicology, Centre for Environmental Sciences, Hasselt University, Campus D – B3590 Diepenbeek,

*Running title: *The effect of nanoparticles on osteogenesis*

To whom correspondence should be addressed: Smeets Karen, Tel: +32 (11) 26 83 19; Email: karen.smeets@uhasselt.be

Keywords: Nanoparticles, Osteogenesis, Stem cells, Developmental processes, Mitochondria

ABSTRACT

Nanoparticles (NPs) are widely implemented in daily life applications (1-3). However, exposure to NPs is of major concern for human health, particularly with respect to developmental processes. In this research, human dental pulp stem cells were used as a proxy for mesenchymal stem cells to investigate the effects of three broadly used NPs, silver (Ag), titanium dioxide (TiO_2), and polystyrene (PS). NP characterization was performed with dynamic light scattering. Nanoparticle-specific effects on the differentiation capacity of stem cells were investigated by the observation of the amount of calcium deposition with Alizarin red S combined with cetylpyridinium chloride. Also, mitochondrial parameters were studied since these organelles play a central role in osteogenesis. Here, mitochondrial morphology and physiology changes due to NP exposure were assessed by confocal microscopy and JC-10 assay.

Results indicated that AgNPs affect the mitochondria and the differentiation capacity. Mitochondria were less abundant, and their morphology appeared swollen compared to the other NP exposures. Further AgNP exposure caused a decrease in osteogenesis, while TiO_2NPs induced differentiation. However, both Ag and TiO_2NPs resulted in cell death at higher concentrations. Regarding PSNPs, exposure did not negatively affect the cells. Though, depending on the cell's age, results suggest that older cell passages lose some ability to cope with the possible nanoparticle-induced stress. NP exposure affects the developmental processes, potentially via alteration of the mitochondrial functioning. Further research could use these results of mitochondrial parameter changes to investigate their use in biomarker development and risk assessment strategies.

INTRODUCTION

The implementation of nanoparticles (NPs) in everyday applications is increasing strongly and varies from medical devices to food additives (1-3). Furthermore, NPs end up in the environment due to industrialization and domestication, resulting in human exposure via several routes such as the gastro-intestinal tract, transdermal, and the respiratory system (4). However, exposure to NPs is of major concern, particularly with respect to developmental processes. Knowledge about the use of NPs in the developmental processes is still lacking, mainly because researchers focussed on the effect of NPs on differentiated cells. Limited studies focused on the exposure effects of NPs on stem cells. Stem cells drive the development and maintenance of early and of adult human life. Mesenchymal stem cells (MSCs), for example, are a heterogeneous population of stromal cells found in the umbilical cord, bone marrow, and menses blood (5, 6). They are characterized by two key features they are self-renewing and can differentiate into different cell lines, e.g. osteogenesis, the formation of bone (7, 8). Since stem cells regulate the development of tissues, it is important to understand how these new pollutants could influence these processes.

NPs have a size range between 1-100 nm (9). The abundant use of NPs in various applications results from their unique characteristics, especially

their small size and consequently large surface-to-volume ratio, resulting in a higher reactivity than larger compounds (10). Other physicochemical properties of NPs that affect their reactivity are, e.g., surface composition, surface charge, shape, and composition, and each of these properties could influence the possible toxicity of the NPs (11).

Three types of abundantly used NPs are titanium dioxide (TiO_2), silver (Ag), and polystyrene (PS) NPs. TiO_2NPs are used in a variety of products ranging from paints to personal care products. They are added to sunscreens, for example, because TiO_2NPs can block ultraviolet radiation (12). Further, TiO_2NPs contain a white color, which causes them to be used as a food additive (E171) (2). Overall, TiO_2NPs are considered to be inert (13), indicating that the interaction with biological material is minor. However, several studies indicated that TiO_2 could induce reactive oxygen species (ROS) and deplete cellular antioxidants, causing adverse biological effects such as lipid peroxidation and DNA damage (14).

PS is one of the most used polymers in plastics, specifically in food packaging (15). A part of these packages could end up in the environment, specifically the open waters. Through several processes, the larger plastic fragments will be degraded to NPs (16, 17). Aquatic organisms are then directly and indirectly exposed to these NPs, which results in the entry of PSNPs into the food chain (18, 19). Through the biocompatible characteristics of PSNPs, adverse effects on biological systems are expected to be limited (20). Although their inert properties, adverse health effects are observed both *in vivo* and *in vitro*. For example, PSNP exposure could cause an accumulation in the organs, leading to ROS formation and a disturbance in energy balance (21, 22).

Overall, AgNPs are incorporated in products because of their antibacterial properties, for example, in food packaging, textile, and medical equipment (3). AgNPs are considered highly reactive since they can release Ag^+ ions, which interact with and damage cell structures (14). This release could further lead to the formation and accumulation of ROS inside the cell (23). Studies on the toxicity of AgNPs showed that AgNP exposure could cause genotoxic effects when entering the mammalian cell. *In vivo* studies showed that AgNP exposure could damage different organs such as the central nervous and respiratory systems (14).

Literature showed that a common effect of NP exposure is the production of ROS, small oxygen-containing molecules which can interact with biological systems (14, 21, 23, 24). This accumulation of ROS, such as hydrogen peroxide (H_2O_2), contains an additional electron, which makes these molecules reactive toward various chemical structures such as DNA (24). However, the cell contains a defense mechanism, namely antioxidant enzymes, to cope with stress and avoid damage (25).

In healthy cells, ROS also has an important signaling role in a variety of processes such as the cell cycle and differentiation (24, 26, 27). Therefore the induction of oxidative stress could disrupt the osteogenesis capacity of the cell (24). More specifically absence of ROS stimulates osteogenesis, while the presence could inhibit it (24). Different studies on the effects of NP exposure on stem cells observed that exposure resulted in ROS formation leading to a decrease in osteogenesis (13, 23, 28). Researchers observed that levels of intracellular ROS are decreased together with an upregulation of protein subunits of respiratory enzymes, the number of mitochondrial DNA (mtDNA), oxygen consumption rate, and antioxidant enzymes (29). Furthermore, they noticed that higher levels of ROS stimulated the differentiation toward adipogenesis (21, 24).

ROS could be induced by NP exposure, although the mitochondria are the central organelle in the cell that produces ROS, for example, as a by-product of mitochondrial metabolism and cellular respiration (24). Mitochondria have an essential role in the differentiation capacity of stem cells. For example, they provide the cell with energy during differentiation (30, 31). During this process, an increase in mitochondria biogenesis is observed, followed by an elongation of the organelle, known as fusion, as well as an increase in the number of cristae (31, 32). In contrast, the fission of the mitochondria is a characteristic for other differentiation processes like chondrogenesis or mitotic transition (32, 33).

Furthermore, the mitochondria can promote osteogenesis in stem cells by the bioenergetic process of oxidative phosphorylation. Glycolysis is the main energy source of undifferentiated cells, but

once the mitochondrial energy production is changed to oxidative phosphorylation, it can promote differentiation in hMSCs (29). To be specific, during this process, the production of acetyl-COA occurs, which can activate β-catenin by acetylation (30). This in turn, works as a transcription factor and causes the transcription of runt-related transcription factor 2 (RUNX2), the master regulator of osteoblast differentiation (34, 35). Once RUNX2 is activated, the stem cell will be classified as a preosteoblast, and the differentiation towards a mature osteoblast start (34). After this activation, the preosteoblast will undergo a three-stage differentiation. Stage one is the proliferation stage. In stage two, the differentiation starts, and lastly, stage three, where mineral deposition of mineralization, e.g., calcium deposition, starts (34).

NP exposure to stem cells could induce oxidative stress that leads to ROS production (13, 14, 21-23, 28). However, different particles can induce different effects (36). So it is needed to understand how NP exposure can influence the regulation of the developmental processes, such as mitochondrial functioning, since the mitochondria play a key role in the differentiation by providing the cell with energy and regulating the differentiation. Here I expect that alterations in the mitochondrial functioning due to NP exposure could alter the differentiation capacity of the MSCs. In this research, the effects of three different NPs on the differentiation capacity of MSCs will be investigated. Human dental pulp stem cells (hDPSCs) extracted from wisdom teeth will be used as a proxy for MSCs to study the effects of NP exposure on the osteogenesis capacity of stem cells. Three commonly used types of NPs are used: TiO_2NPs, PVP-AgNPs, and COOH-PSNPs. I hypothesize that TiO2, Ag, and PSNP exposure in hDPSC will result in mitochondrial dysfunction due to oxidative stress, leading to alterations in the osteogenic capacity of hDPSC. The hypothesis of this study will be investigated with three aims. First, the characterization of the NPs, to better understand the interaction of the NPs with the hDPSCs. Second, the impact of NP exposure on the osteogenesis capacity of the hDPSCs. Osteogenesis will be induced with or without NPs, and the osteogenesis capacity will be studied in a quantitative and qualitative manner. Furthermore, osteogenesis-related genes were selected, primers were designed, and efficiency was tested for RT-qPCR. Lastly, the effect of NP exposure on mitochondrial functioning was studied. Morphological and physiological changes in the mitochondria were investigated. These results are linked to the characterizations of the three different NPs to find a link between the characteristics of the NPs and the alterations in mitochondrial functioning and osteogenesis processes.

EXPERIMENTAL PROCEDURES

Cell culture – hDPSCs were provided by BIOMED (Hasselt, Belgium). The cells were cultured in a T25 cell culture flask (Greiner Bio-One GmbH) containing complete cell medium, which is 5 mL minimum essential medium (α-MEM, Gibco) supplemented with 10% heat-inactivated fetal bovine serum (FBS, Sigma Life Science), and 1% penicillin/streptomycin (pen/strep, Gibco). The cells were kept at 37 °C in a 5% CO_2 atmosphere incubator (Binder GmbH). Medium was changed twice a week. At 70-80 % confluence, cells were harvested for re-culturing or seeding for experiments. Cells were washed twice with Phosphate Buffer Saline (PBS, without calcium chloride and magnesium chloride, Gibco, Life Technologies) followed by addition of 0,05% Trypsin-EDTA (Gibco, Life Technologies) for 5 – 8 min (37 °C, 5% CO_2). The enzymatic effect of Trypsin-EDTA was stopped by the addition of complete cell medium and the cells were pelleted by centrifugation (5 min, 300 g, 21 °C). After counting the cells using Trypan-blue (Gibco, Life Technologies) the pellet was resuspended in complete medium (1 million cells/ml). Cells were either seeded or frozen. Only cells between passage 6-10 were used during the different experiments

Characterization of nanoparticles – The following NPs were commercially purchased: 21 nm spherical TiO_2NPs (Degussa Evonik GmbH, powder), spherical COOH-PSNPs (10% w/v) of 63 nm (Magsphere) and PVP-AgNPs with a spherical shape and a size of 20 nm (US Research Nanomaterials Inc.). NP stocks were made in autoclaved filtered MilliQ (filter pore 2 µm) and sonicated in a water bath sonicator (Ultrasonic Cleaner USC-TH, VWR) for 15-20 and 30 min at 37 kHz for Ag and TiO_2NPs respectively. Before each experiment new Ag and TiO_2NPs stocks were made. A PSNPs stock was made once, sonicated for 15 min in a water bath sonicator (37 kHz) and used

during all experiments. Before use, the stock was vortexed for 30 sec. The actual size of Ag and TiO2NPs was verified in a previous study of our research group using transmission electron microscopy (TEM). To confirm the characterizations of the manufacturer, the hydrodynamic diameter and zeta potential of the NPs were measured via dynamic light scattering measurements (DLS) with the ZetaSizer Nano (Malvern Panalytical). Before measurements NPs were dispersed in either 1 mM NaCl-solution, or in MilliQ and osteogenesis medium (complete cell medium supplemented with 5 % StemXVivo Human osteogenic Supplement (R&Dsystems)) in a 10 µg/ml concentration, for zeta potential and hydrodynamic size respectively. Measurements were performed at room temperature.

Analyzing osteoblast differentiation with Alizarin red S staining – At 50-70 % confluence osteogenesis was induced by treating the cells with osteogenesis medium. Osteogenesis medium was refreshed twice a week. To verify osteogenesis, Alizarin red S (ARS) assay was performed to observe calcium formation, which is an indication of osteoblast differentiation. In short; cells were washed twice with dH_2O_2 and stained with 40 µM filtered ARS (pH= 4.3) (Thermo Scientific) for 15 min at RT. Cells were washed four times with dH_2O_2 and visualized with an inverted microscope (Nikon DS-Fi3). Calcium quantification was performed by eluting the bound ARS in 10% Cetylpyridinium chloride (CPC) (Sigma-Aldrich) in 10 mM sodium phosphate for 15 min. Absorbance was measured at 550 nm with the spectrophotometer (FLUOstar Omega, BMG LABTECH). The first time a wide range of conditions was screened namely: control with osteogenesis medium (C+), control with only cell medium (C-), 1, 5, 10, 25, and 50 µg/ml for AgNPs, 10, 25, 50, 100, and 250 µg/ml for PSNPs and 10, 50, 100, 175, and 250 µg/ml for TiO_2NPs. A second experiment was performed for a validation of selected conditions: C+, C-, 1 and 10 µg/ml for AgNPs and 10 and 100 µg/ml for TiO_2 and PSNPs. For both experiments, the following three time points were selected: 3,7, and 14 days.

JC-10 assay for membrane potential measurement in differentiating hDPSCs – JC-10 assay was performed in order to analyze the effects of NP exposure on the mitochondrial membrane potential. Approximately 1.7 x 10^3 cells were sown in a black 96-well plate. After three days of growth, osteogenesis was induced for a duration of 3 or 7 days, by the addition of osteogenesis medium with or without NPs. The following conditions were applied C+, C-, 1 and 10 µg/ml AgNPs and 10 and 100 µg/ml TiO_2 and PSNPs. Carbonyl cyanide m-chlorophenyl hydrazone (CCCP, 50 µM, 37 °C) was used as a positive control and added 4 h before the end of the exposure. All cells were washed twice with Dulbecco's Phosphate Buffered Saline (with calcium and magnesium, DPBS, Gibco, Life Technologies). Next, 5 µM JC-10 (Enzo Life Sciences) diluted in DPBS was added and incubated for 30 min (37 °C, 5% CO_2), followed by three washing steps with DPBS. Fluorescence was measured at 590 nm (orange spectrum) and 520 nm (green spectrum) using a FLUOstar Omega spectrophotometer (BMG LABTECH) at 590 nm (orange spectrum) and 520 nm (green spectrum). The ratio of orange/green fluorescence was determined and compared to the C+ values.

MitoTracker™ Red CMXRos for visualizing active mitochondria with confocal microscopy – To study the effect on the morphology of the mitochondria after NP exposure, cells were stained with MitoTracker™ Red CMXRos (Ex/Em 579/599, Life Technologies). 1 x 10^4 cells were seeded in a 24-well plate on coverslips and grown for 3 and 7 days after osteogenesis induction with or without NP exposure. 1 and 10 µg/ml AgNPs, and 10 and 100 µg/ml TiO_2 and PSNPs. Cells were washed two times with DPBS and stained for 30 min with 250 nM MitoTracker CMXRos diluted in DPBS (37 °C, 5% CO_2). Next, the cells were fixed in 4% paraformaldehyde (PFA) diluted in DPBS (15 min, RT), followed by two washes with DPBS and addition of counterstaining of 1.33 µM Hoechst 33342 (Ex/Em 361⁄497, Invitrogen by Thermo Fisher Scientific) in DPBS (13 min, RT). Finally, the cells were washed three times with DPBS and mounted on glass slides with Slow fade (Invitrogen by Thermo Fisher Scientific). Samples were visualized with confocal microscopy (Zeiss – LSM900 KMAT) and Zen blue 3 software. In each sample, three different regions were imaged, using a 40x water objective (LD C-Apochromat 40x/1.1 W) and lasers 561 nm and 405 nm for MitoTracker Red CMXRos and Hoechst 33342 respectively,

creating a 3 by 3 tile scan. Out of the high resolution tile scan, representative cells are selected and used for analysis. Images were analyzed using the Skeletonized feature in ImageJ, to visualize mitochondrial structures as described by Valente A. et al. (37)

Gene selection and primer design – An in depth literature study was performed to gather knowledge about the different genes, which interact with the different processes of osteogenesis. Primers were designed using Primer3 software with the following parameters: a product size between 70-150 bp, primer size between 18-25 bp, primer Tm between 57-63 °C, max Tm difference 1°C, % GC between 20-80 % max self-complementarity 5 or below and max 3' self-complementarity as low as possible. A selection of possible primers was verified with NCBI primer blast to control for a 100 % coverage, product length and products on target template. The selected primers were manufactured by Biolegio (table S1).

Sample collection and primer efficiency testing – Real-Time quantitative PCR (RT-qPCR) was used to test the efficiency of the designed primers on mixed-samples, that were created of final cDNA samples (as described in supplement). A two-fold serial dilution ranging from 28 – 0,4375 ng/µl was prepared in RNase free H_2O. RT-qPCR was performed in a 384-well plate using the QuantStudio™ 5 Real-Time PCR System (Thermo Fisher Scientific) with the following settings: 20 sec at 95 °C, 40 cycles of 1 sec at 95 °C, and 20 sec 60 °C. SYBR® Green Master Mix was added to the diluted cDNA samples and containing 5 µL Fast Sybr Green (Applied Biosystems, ThermoFisher Scientific), 0,3 µL for both 10 µM forward and reversed primer, and 1,9 µL RNase free water. Analysis was done with the QS5 analysis software (Thermo Fisher Scientific).

Statistical analysis – R version 4.2.0 with Rstudio desktop version 2022.02.2+485 was used to perform statistical analysis with significance level 5%. Outliers were detected with the Cook's distance test with cd > 1. With the Shapiro-Wilk test and Barlett's test were respectively the normal distribution and homoscedasticity of the data verified. Data was transformed (logarithm, square root, inverse or exponential) if needed. When data meets the two assumptions a two-way ANOVA with *post-hoc* Tuckey-Kramer was performed. In the case of a violation of normality or homoscedasticity, the non-parametric test, Kruskal-Wallis with *post-hoc* Wilcoxon rank sum was performed.

RESULTS

Characteristics of the different nanoparticles – The hydrodynamic size of the three particles was measured in MilliQ and osteogenesis medium. For AgNPs the majority of the NPs had a hydrodynamic size of 882.8 ± 436.4 nm in osteogenesis medium and 441.0 ± 14.15 nm in MilliQ. For TiO_2NPs this was 354.0 ± 133.5 nm and 559.8 ± 76.51, and for PSNPs 111.4 ± 60.56 nm and 70.46 ± 22,87 nm (table 1). Furthermore, the polydispersity index (PdI) was studied. Depending on the solution, the PdI value changed. For AgNPs, the PdI was 0.809 in MilliQ and 1.00 in osteogenesis medium. For TiO_2NPs the PdI value were 0.586 and 0.612, respectively and for PSNPs the PdI values were 0.180 and 0.619 (table 1).

The zeta potential was measured two times for Ag and TiO_2NPs. For the AgNPs, the results between different measurements differ. For the first stock, the zeta potential was -24.00 ± 8.54 mV, and for the second measurement, -7.97 ± 8.54 mV (table 2). In the case of TiO_2NPs, the zeta potential was similar for the two different measurements; this was approximately -29 mV for both measurements (table 2). The zeta potential for PSNPs was not measured in NaCl.

Calcium nodules are stained with ARS staining – The osteogenesis capacity of hDPSCs after NP exposure was investigated with ARS staining. ARS is a staining that binds to the calcium nodules formed by the cell, which is an early indication of osteogenesis. Visual inspection with ARS staining after 3 and 7 days of osteogenesis induction showed for C+ and C- red stained calcium nodules (fig 1.E, 1.F), which were not visualized after 14 days.

After 3 days of osteogenesis induction, no calcium nodules were observed for the three different NPs. In the case of AgNPs, stained nodules are visualized after 7 days of 1 and 10 µg/ml AgNP exposure. Clear red calcium nodules were visualized only for the lowest concentration of AgNPs after 14 days of exposure (fig 1.I). The TiO2NPs exposed cell layer appeared red when

Table 1 – Size of the three studied NPs: Particle size (in nm) according to the manufacturer and validated with transmission electron microscopy (TEM). Hydrodynamic average size (Z-average) of the nanoparticles (NPs) measured in MilliQ (MQ) and in osteogenesis medium. Intensity (in %) which refers to the majority of the cells in a certain size range. Polydispersity index (PdI) show the distribution of the particles in a certain solution. Data are expressed as mean ± SD

	Manufacturer	TEM	DLS (in MQ)		DLS (in Osteogenesis medium)		
NP	Particle size (nm)	Particle size (nm)	Z-average (nm)	PdI	Hydrodynamic size (nm)	Intensity (%)	PdI
PVP-Ag	20	33 ± 14	441.0 ± 14.15	0.809	882.8 ± 436.4	52.3	1.000
TiO2	21	24 ± 8	559.8 ± 76.51	0.586	354.0 ± 133.5	84.3	0.612
COOH-PS	63	/	70.46 ± 22,87	0.180	111.4 ± 60.56	74.7	0.619

inspected with the naked eye. However, after visualization with the microscope, no individual stained nodules could be observed for the different NP concentrations or exposure durations (fig 1.H). In the case of PSNP exposure, after 7 days of exposure, stained calcium nodules were present for both 10 and 100 µg/ml PSNPs. More prominent stained calcium nodules could be visualized after 14 days of 100 µg/ml PSNPs (fig 1.G). These were not visible for the other NP concentrations or exposure durations.

To quantify the formation of calcium, the ARS staining was eluted using CPC. After 3 days of osteogenesis induction with AgNPs, an increase in osteogenesis was observed, followed by a decrease in osteogenesis (seen after exposure to 10 µg/ml AgNPs and higher). A significant ($p = 0.0427$) increase in calcium formation was observed after exposure to 1 µg/ml AgNPs for 3 days compared to the C+. Furthermore, a significant decrease ($p = 0.0121$) in calcium formation was observed after 3 days of 50 µg/ml AgNP exposure compared to the C+ (fig 1A). After 7 days of osteogenesis induction, a decrease in calcium formation was observed for the three higher AgNP concentrations. Which was significant only for 25 and 50 µg/ml ($p = 0.0061$ and $p = 0.0179$ respectively) compared to C+. The same effect was observed after 14 days of osteogenesis induction; 25 µg/ml resulted in significantly less calcium formation compared to C+ ($p = 0.0106$). Exposure duration influenced the calcium formation too, 3 days of 1 and 25 µg/ml AgNP exposure resulted in more calcium nodules compared to 7 days ($p = 0.0404$ and 0.0286) (fig 1A). Further, 14 days of 50 µg/ml AgNP exposure showed significantly less differentiation compared to 3 days 50 µg/ml AgNP exposure ($p = 0.0294$) (fig 1A).

TiO2NP exposure resulted in a non-significant upwards trend of calcium deposition, with increasing NP concentration for all conditions. After 3 days, only 100 µg/ml TiO2NP exposure resulted in a significant increase ($p = 0.02051$) in osteogenesis compared with the C+. A decrease in calcium formation was seen after 50 µg/ml TiO_2NP exposure compared with the C+ and other exposure conditions after 3 days. However, after 7 and 14 days of exposure, calcium levels were increased for several of the exposure concentrations. 50, 175, and 250 µg/ml ($p = 0.01212$, 0.00606, and 0.00606) of exposure resulted in a significantly increased absorbance after 7 days, while after 14 days 100, 175, and 250 µg/ml ($p = 0.04009$, 0.00606, and 0.00606) showed a significant increase in absorbance compared to the C+ (fig 1B). While the lower concentrations of TiO_2NPs resulted in less calcium formation compared to C+ (fig 1B). When comparing the different time points, it could be concluded that 7 and 14 days had higher calcium levels than 3 days of exposure (fig 1B).

Significant less calcium formation was observed after 3 days of 5 and 250 µg/ml ($p = 0.0427$ and 0.0121, respectively) PSNP exposure compared to the C+. After 10 and 100 µg/ml PSNP exposure, an increasing trend was observed; after 50 µg/ml PSNP exposure, a decrease in osteogenesis was observed. After 7 days of PSNP exposure, only the two highest concentrations showed a significant increase in osteogenesis compared to the C+ ($p = 0.0061$ and 0.0179). After 14 days of osteogenesis induction, exposure to 100 µg/ml PSNPs showed a significant increase ($p = 0.0106$) (fig 1C). Significant increase in calcium nodules was visible between 3 and 7 days of PSNP exposure. After 3 days of 5 and 100 µg/ml, PSNP exposure had significantly more calcium formation

Table 2 – Zeta potential of the three studied nanoparticles measured in NaCl and expressed as mV ± SD.

Nanoparticles (in NaCl)		Zeta Potential (mV)
PVP-Ag	Stock 1	- 24.00 ± 8.5
	Stock 2	- 7.97 ± 3.73
TiO_2	Stock 1	- 29.20 ± 5.03
	Stock 2	- 29.2 ± 4.18
COOH-PS	/	/

(p = 0.0404 and 0.0286) compared to 7 days of exposure. For a concentration of 250 µg/ml PSNPs significantly more calcium formation was observed after 14 days compared to 3 days (p = 0.0294) (fig 1C).

The effect of cell passage on the differentiation capacity – The formation of calcium nodules during osteogenesis was examined in two independent experiments performed on two different cell passages (#). Two selected concentrations were tested per NP. A comparison of the overall effects for each of the different cell passages showed that longer osteogenesis induction resulted in more calcium formation for #7, while the increase over time was not present for cells of #10. In general, this was visualized for C+ and all NP exposures (fig 1.D). Furthermore, it was observed that for #10, a less dense layer of cells was present in the wells compared to the younger passage (#7).

The quantitative data corroborated the qualitative data since less calcium formation was observed for #10 compared to #7 (fig 1.D). Exposure to 10 µg/ml AgNPs for 3 and 7 days, resulted in significant more calcium formation for #10 compared to #7 (p = 0.029 and 0.029 respectively) (fig 1.D). For TiO2NPs, a significant increase in calcium formation is observed for #10 compared to #7 after 3 days of 10 µg/ml (p = 0.029) and 100 µg/ml (p = 0.029) TiO2NP exposure. In the case of PSNPs, a different effect was visible. After 3 days of PSNP exposure, significantly more calcium formation was observed by #10 compared to #7 for both concentrations (p = 0.029 and 0.029). While by 7 and 14 days, the opposite was observed. After an exposure of 10 µg/ml PSNPs, a significant decrease in calcium formation was noticed for #10 compared to #7 after 7 and 14 days of exposure (p= 0.029 and 0.029, respectively). A decrease in calcium formation was observed after 100 µg/ml PSNP exposure for 14 days for #10 compared to #7 (p=0.029) (fig 1.D).

Mitochondrial membrane potential changes after nanoparticle exposure during differentiation – Mitochondrial membrane depolarization indicates possible damage to the mitochondria. This was studied with the fluorescent dye JC-10 at two time points: 3 and 7 days after osteogenesis induction with or without NP exposure. Results after 3 days of NP exposure, showed no significant differences for the different NP conditions with the C+ (fig 2). However, a decreasing trend of the 590/520 ratio was observed for all NP conditions, CCCP, and C+, compared to C- (fig 2). Between the two concentrations per NP, no significant increase or decrease is observed after 3 days of NP exposure (fig 2). Nevertheless, with increasing AgNP concentration, membrane depolarization occurred, while the opposite was observed between the two PSNP exposure (fig 2). However, these differences were not significant.

After 7 days of NP exposure, a significant increase in 590/520 ratio was detected in C- (p = 0.0087) and 10 µg/ml AgNP exposure (p = 0.026), and a significant decrease in 100 µg/ml PSNP exposure (p = 0.026) compared to C+ (indicated with #). Furthermore, after 7 days of osteogenesis induction with AgNPs, an significant increase in membrane polarization was observed after 10 µg/ml compared to 1 µg/ml AgNPs (p = 0.026). A significant depolarization occurred after 100 µg/ml TiO_2NP exposure compared to 10 µg/ml TiO_2NPs (p = 0.0152). After exposure to 100 µg/ml PSNPs a stronger depolarization of the mitochondrial membrane occurred compared to 10 µg/ml PSNPs (p = 0.026) (fig 2).

No significant differences were observed between 3 and 7 days of osteogenesis induction with or without NPs. In general, after 7 days, a higher 590/520 ratio was observed than after 3 days; this was most visible by 10 µg/ml of AgNP exposure (fig 2).

Mitochondrial morphological changes after nanoparticle exposure – MitoTracker Red is a staining that visualizes the cell's active mitochondria, which accumulation depends on their mitochondrial membrane potential. Samples of the cells were prepared after 3 days and 7 days of NP exposure. Mitochondrial morphology of C+

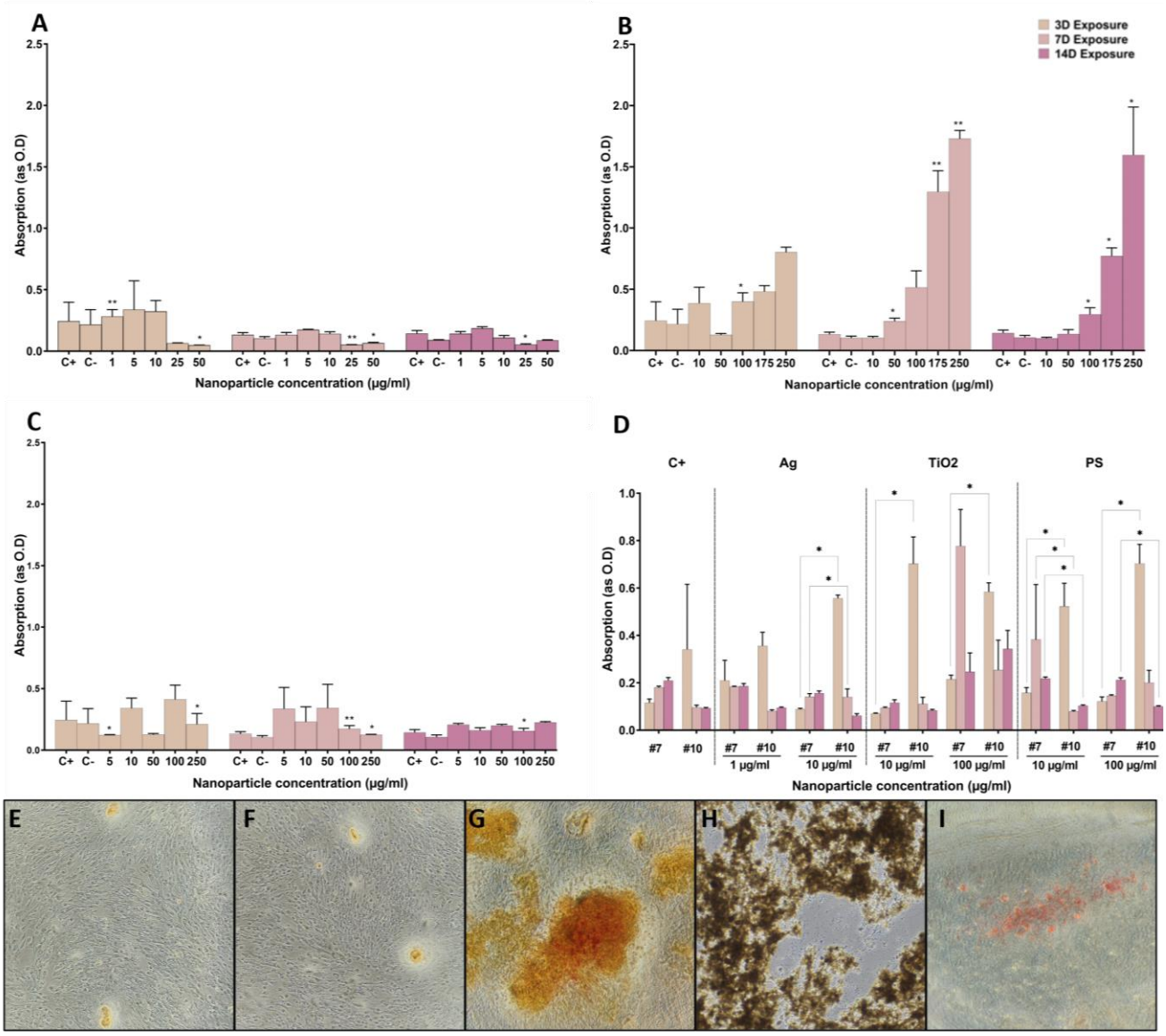

Figure 1 – Calcium formation during osteogenesis: The formation of calcium was observed to study the effect of NP exposure on the osteogenesis capacity of hDPSCs. **A**. Effect of AgNPs on calcium formation **B**. Effect of TiO_2NPs on calcium formation **C**. Effect of PSNPs on calcium formation. **D**. Effect of passage number on the calcium formation, where passage number is indicated as (#). Visualization of stained calcium nodules is visualized by the following figures: **E**. C+ 3 days of osteogenesis induction **F**. C- 3 days of osteogenesis induction **G**. 100 µg/ml PSNP exposure after 14 days **H**. 100µg/ml TiO_2NP after 14 exposure days I. 1 µg/ml AgNP exposure after 14 days. Images are made with inverted microscopy (Nikon DS-Fi3). Results are expressed as mean values + SD, n = between 4 or 8. Significant results are indicated with * < 0.05, ** < 0.01 and *** < 0.001

showed for both 3 and 7 days tubular shape and a diameter of approximately 1 µm throughout the cell. The mitochondrial network was denser after 7 days of osteogenesis induction compared to 3 days (fig 3.D, S1.D, and S2.D). After 3 days of osteogenesis induction, swollen mitochondria were observed with a size of ~ 1.25 µm, which was not the case after 7 days. (fig S2.D3, D4, white arrow). PSNP exposure showed for both 10 and 100 µg/ml PSNPs, equivalent mitochondrial morphology compared to the C+ for both time points. However, after 100 µg/ml PSNP exposure for 3 and 7 days, some thickening (~ 0.8 µm) of mitochondria was visible (fig 3.A3, A4, and fig S2.A4, white arrow). After 10 µg/ml exposure for 7 days, long tubular mitochondria were observed together with swollen structures (~ 1.5 µm) that showed less intense fluorescent staining (fig S1.A3).

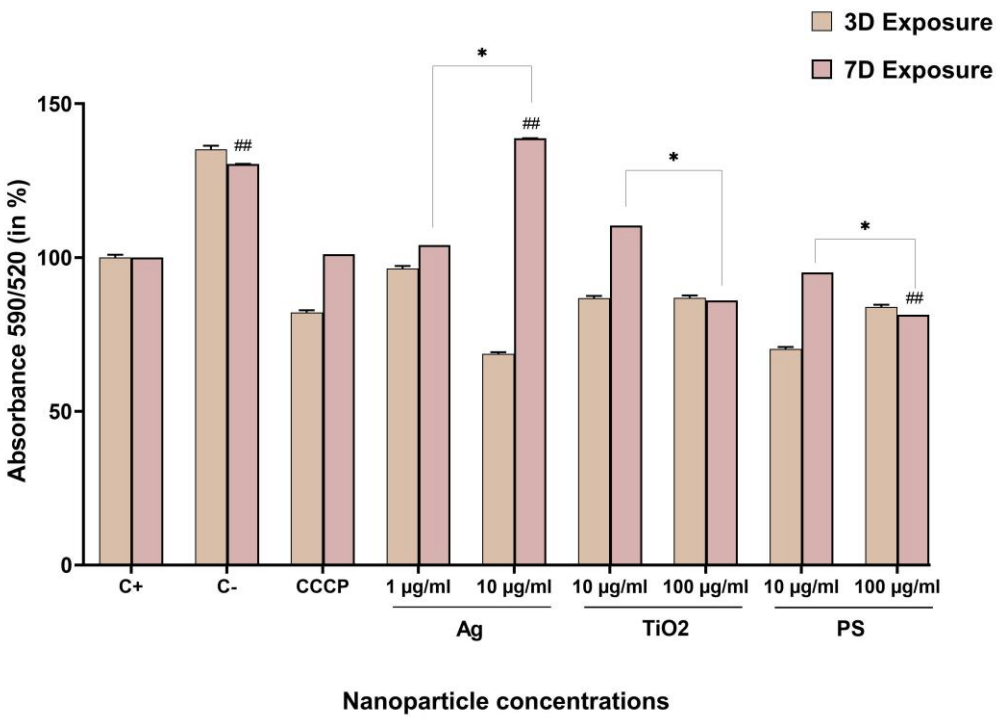

Figure 2 – Indication of mitochondrial membrane damage with JC-10 assay: Effect of NPs (Ag, TiO_2 and PSNPs) exposure on the mitochondrial membrane potential after 3 and 7 days of exposure. Values are the ratio of 590/520, expressed in % + SD were C+ is set as 100 %, n = 6 from one independent experiment., Significant differences between different concentrations are indicated as * < 0.05, ** < 0.01 and *** < 0.001. Significant differences with the C+ after 7 days are indicates with # < 0.05, ## < 0.01 and ### < 0.001

Exposure to 10 µg/ml AgNPs for both 3 and 7 days, results in smaller and fragmented mitochondria (yellow arrows) and short, swollen mitochondria of ~1.4 µm (blue arrows) compared to C+ (fig 3.B, S2.B). Exposure of 1 µg/ml AgNPs for 7 days showed less swollen mitochondria compared to 100 µg/ml AgNP exposures. Fragmentation of the mitochondria was still present but less pronounced as compared to 100 µg/ml AgNP exposure (fig S1.B3 and B4, blue arrow and yellow arrow).

TiO2NP exposure resulted in a more extensive mitochondrial network with longer tubular morphology with a diameter of ~ 0.7 µm, and longer branches, this for both 10 and 100 µg/ml TiO_2NP exposure after 7 days, which was more noticeable for the 100 µg/ml TiO_2NP exposure (fig 3C, S1.C, and S2.C). After 10 µg/ml TiO_2NP exposure, tubular mitochondria were observed, but the morphology and density did not differ much from the C+ (fig S1).

Primer design for osteogenesis gene expression – Based on the literature study, osteogenesis-related genes were selected that contributed to the processes of osteogenesis and mitochondrial processes. These genes were: RUNX2, Osteocalcin (OCN), Alkaline Phosphatase (ALP), Osteopontin (OPN), Collagen type I alpha (COL1A1), Osterix (Sp7), β-catenin, WNT Family Member3A and 5A (WNT3A and WNT5A). Further, mitochondrial genes that are linked to osteogenesis are selected. These were (MFF), OPA1 Mitochondrial Dynamin Like GTPase (OPA1), and Mitochondrial fission protein 1 (FIS1). Oxidative stress genes were also selected to study the possible upregulation of the antioxidant genes due to the induction of oxidative stress due to NP exposure. The following genes were chosen: Glutathione peroxidase 4 (GPX4), Glutathione peroxidase 1 (GPX1), Glutathione-disulfide reductase (GSR), Catalase (CAT), Superoxide dismutase 1 (SOD1).

Primers that fulfill the different parameters in Primer3 were verified in NCBI primer blast to control for 100 % coverage with the target gene and right product length.

Testing primer efficiency of the designed primers – Primers were tested a first time on mixed samples (1 and 10 µg/ml AgNPs, 10 and 100 µg/ml TiO_2 and PSNPs, C+ and C-, for different exposure durations), and efficiency was calculated (table S1). Based on the calculation of the efficiency and melting curve, two osteogenesis genes were selected, COL1A1 (efficiency 104,91 %) and β-catenin (efficiency 91,37 %), and one mitochondrial related primer MFF (efficiency

104,19 %). GPX1 (efficiency 94,48 %), GSR (efficiency 91,57 %) and SOD1 (efficiency 91,83 %) were selected for the oxidative stress genes (table S1). A small selection of the primers (RUNX2, ALP, OCN, COL1A1) was re-tested on mixed samples from different control conditions. Only results were obtained with COL1A1 (with an efficiency of 75.86 %). For the other genes, the primers did not bind (data not shown).

DISCUSSION

Possible formation of protein corona in osteogenic medium – Depending on their characteristics, NPs are selected for specific applications. Characteristics of the NPs were investigated by measurement of the hydrodynamic size and zeta potential. The hydrodynamic size of the NPs was measured in a 10 µg/ml concentration in osteogenesis medium and in MilliQ and indicates how the particles behave and interact in a fluid (38, 39). The zeta potential of the particles is an indication of their stability and surface charge. Particles with an (absolute) value of ± 30 mV or higher are considered stable particles, which means that the chance of interaction between NPs is unlikely (40). On the contrary, a zeta potential between ± 0 – 10 mV indicates highly unstable particles (40).

Depending on the medium, the hydrodynamic size of the NPs differs. TiO_2NPs have a hydrodynamic size of approximately 354 nm and 559 nm in osteogenesis medium and MilliQ, respectively (table 1). These values are higher than the manufacturer's stated size of 21 nm and the 24 nm measured with the TEM (table 1). This suggests that proteins in the osteogenesis medium are bound to the NP surface, resulting in protein corona and increasing the size of the NPs. However, the larger hydrodynamic size in MilliQ indicates interaction between the NPs. However, TiO_2NPs have a zeta potential of approximately – 29 mV, measured in two independently prepared NP stocks in 1 mM NaCl (table 2). This value indicates that these NPs are stable, and interaction between the NPs is unlikely. The PdI value is an indication of the heterogeneity of a sample in a solution and indirect if particle interaction could occur. Values of > 0.7 are assigned to samples with a broad range of NPs distribution (higher heterogenicity) (41). PdI values of TiO_2NPs are both < 0.7 for the measurements in osteogenesis medium and MilliQ (table 1). The larger hydrodynamic size of TiO_2NPs is due to the formation of protein corona in de case of osteogenesis. Although the value of < 0.7 of PdI, the higher values of hydrodynamic size in MilliQ indicate that there is still an interaction between the TiO_2NPs.

For PSNPs, the hydrodynamic size in MilliQ is close to the size described by the manufacturer (table 1). Here, the PdI is 0.180, which indicates homogeneity and a minor chance of aggregate formation of the PSNPs. In osteogenesis medium, the size of PSNPs is substantially larger, namely 114.4 nm, which is almost double the size stated by the manufacturer (63 nm). For this measurement, the PdI was 0.619, which is < 0.7, implying the homogeneity of the PSNPs in the solution (table 1). However, the larger hydrodynamic size indicates the formation of protein corona.

The hydrodynamic size of the AgNPs is approximately 441.0 and 882.8 nm (table 1). These values are larger than the 20 nm stated by the manufacturer and 33 ± 14 nm observed with the TEM (table 1). Two independent measurements of the zeta potential of AgNPs gave two different values for the zeta potential, -7.97 ± 3.73 mV and -24.00 ± 8.50. The large difference between the two measurements could be due to the variation between the AgNPs stocks. Furthermore, the value of -7.97 ± 3.73 mV indicates instability of AgNPs, and interaction between the AgNPs (table 2). The PdI of AgNPs was for both mediums > 0.7, which indicates of heterogeneity and the chance of aggregate formation (table 1). Further, the large value of the hydrodynamic size of AgNPs could be linked to the formation of protein corona in the osteogenesis medium.

TiO_2NPs caused cell death, while AgNPs reduced differentiation and PS did not influence on the osteogenesis capacity – Humans are directly and indirectly exposed to different types of NPs in different ways. NP exposure could lead to oxidative stress and ROS production (13, 14, 21-23, 28), which also could influence the developmental processes in stem cells. In the light of differentiation, the effect of three different NPs on the osteogenesis capacity was investigated. ARS staining can bind to the calcium nodules formed by differentiating cells during stage 3 of osteoblast formation (34). ARS assay combined with CPC

enables us to quantify the ARS that was complexed with calcium via spectrophotometry.

Data of osteogenesis induction for C+ showed a downtrend in calcium formation through time. However, it was expected that more calcium formation was formed after 14 days of osteogenesis induction. This is because following the manufacturer's instructions of the StemXVivo supplement; osteoblasts should be formed after 14 days of osteogenesis induction. The reason for the delay in osteoblast formation could be that hDPSCs need a longer period of incubation.

Overall, TiO_2NPs are considered an inert materials (13). Nevertheless, hDPSCs exposed to TiO_2NPs showed an increasing trend of osteogenesis with increasing concentrations of NPs for all three exposure durations (fig 1). However, a significant increase in calcium formation was observed for the highly TiO_2NP concentrations compared to the C+ (fig 1B). These results indicate that exposure to TiO_2NPs can induce the differentiation capacity of stem cells. However, a study by Ren Y. et al., studied the effect of ~ 80 nm spherical TiO_2NPs on MC3T3-E1 cells (mouse proteoblast). The results of this study showed a negative correlation with osteogenesis. More specifically, apoptosis and obstruction of bone formation were observed (42). The same was observed in a study performed by Hou, Y. et al. who studied the effect of three different TiO_2NPs (no uniform shape and sizes 14 nm, 108 nm, and 196 nm) on the differentiation capacity of MSCs. They show a significant decrease in alkaline phosphatase (an early indication of osteogenesis) with the time of duration and increasing particle size (43).

Several considerations should be made when relating the qualitative results regarding TiO_2NPs, i.e., images acquired of the ARS stained cells, to the quantitative measurements. No cells were visible at the higher concentrations (100, 175, and 250 µg/ml) of TiO_2NPs, but only TiO_2NPs after 7 days of osteogenesis induction (fig1.H). Nevertheless, a red color was clearly visible after ARS staining, and high absorbance could be measured. The measured absorbance is most likely derived from the TiO_2NPs themselves since ARS can be used to fluorescently stain TiO_2NPs (44, 45). Binding of ARS to TiO_2NPs takes place on the hydroxyl group of ARS, which is the same binding place for Ca^{2+}. (46). These findings indicate that TiO_2NPs, in certain concentration ranges, are lethal to the differentiated hDPSCs. A similar result was observed by Ren Y. et al. (42). In my case, cell death could occur due to nutrient deficiency of the hDPSCs since strong deposition of the TiO_2NPs occurred after exposure. After refreshment of the osteogenesis medium, the majority of the TiO_2NPs were not removed, which resulted in a strong accumulation of the TiO_2NPs on the cell layer, and blocked the movement of nutrients to the differentiated hDPSCs. The exact interplay between TiO_2NPs and the observed cell death should be investigated further, e.g., with gene expression. However, in a previous study performed in our research group, the interference between NPs and the absorbance of eluted ARS with CPC. Correction against these results still showed an increase in calcium formation for the different TiO_2NP exposures (data not shown).

Silver is toxic to humans since it can cause ROS due to the release of silver ions (14), which could cause damage to different structures in the cell. Our data showed that osteogenesis was negatively affected by AgNP exposure. This was true for all time points. A decreasing trend is present; however, only the higher concentrations (25 and 50 µg/ml) caused significant reductions in calcium formation compared to C+. However, after 3 days of 1 µg/ml AgNP exposure, significantly more calcium formation was observed. Also, after 14 days of exposure to 1 µg/ml AgNPs, calcium nodules were observed after ARS staining, which was not visible for other AgNP conditions (fig 1.I). Through the toxic characteristics of AgNPs, a decrease or no calcium formation after AgNP exposure was expected, instead of a significant increase of calcium formation compared to C+ (fig 1A). These findings suggest that in lower concentrations, AgNPs could induce osteogenesis somehow. However, another study observed the same effect. Zhang R. et al. studied MSCs with spherical AgNPs with an average size of 10 nm. This NP exposure promoted osteogenesis, probably through the activation of autophagy (47). Further, another study observed that AgNPs (size range between 5 – 15 nm) could induce osteogenesis in MSCs and improve bone fracture healing *in vitro* (48). Although these studies found proof of stimulation of osteogenesis, He W. et al. noticed that AgNP exposure to MSCs resulted in oxidative stress in the inhibition of osteogenesis (23).

However, data were not normalized against the number of cells in each well, which could influence the interpretation of the results. Especially after 7 days of 25 and 50 µg/ml AgNP exposure, no living cells were visible. Here, it is suggested to normalize data in further research, for example, by performing a Bradford assay.

PS is a polymer used in plastics, which is used for food packaging (15). PSNPs could end up in our food in a different way. It is expected that these NPs do not cause adverse effects on biological systems since it is a biocompatible material (20). After induction of osteogenesis with exposure to PSNPs, significant stimulation (100 µg/ml for 7 and 14 days and 250 µg/ml after 3 days) and reduction (5 µg/ml after 3 days and 250 µg/ml after 7 days) of calcium formation was observed (fig 1C). Qualitative data showed that only after 14 days of osteogenesis induction with PSNPs, large calcium nodules were observed (fig 1.G), which was even more abundant than in C+. This indicates that PSNP exposure stimulates osteogenesis since the C+ samples did not show this amount of calcium nodules.

Younger cells could better cope with NPs stress than the older ones – The cell passage number of a cell culture, is the record of times the cell culture has been sub cultured, e.g., harvesting and re-seeding. In this study, hDPSCs are used to investigate the effect of NP exposure on the osteogenesis capacity of stem cells. However, infinite use of these cells is not accepted in research. In general, these cells are used till #10. Researchers observed that top viability was research at #9 (49). Longer use of the cells beyond #15 could result in lower cell viability compared to the younger ones, activation of apoptosis, and a non-significant decrease in cell proliferation (50).

ARS assay was performed twice, once with #7 and the second time with #10. In the first trial with #7, it was noticed that even after NP exposure, the wells were still covered with a layer of cells (in the case of AgNP exposure, the cell layer was less dense but still present). However, when performing the experiment a second time with #10, a large amount of cell loss was observed after 7 days for all NP exposures. Wells were not fully covered anymore for all NPs conditions, and in some conditions, even no cells were present (10 µg/ml AgNPs).

In non-differentiated cells of #10, swollen structures were present together with crystal-like structures (fig S3). Here, we suggest that these swollen structures are differentiated cells, since these stained red after ARS staining. This indicates why more calcium nodules were observed in the second trial compared to the first. These results suggest that younger cell passages could cope better with stress and recover from it by maintaining the proliferation capacity, which is stage one of osteogenesis (34). Older cell passages might have a strongly reduced proliferation capacity, which results in the lack of densely covered wells.

NP exposure reduces mitochondrial membrane potential – Mitochondrial membrane depolarization indicates if potential damage occurred to the mitochondria. As seen in figure 4, mitochondria play an important role during osteogenesis. The effect of NP exposure on the mitochondrial membrane potential was investigated after 3 and 7 days of osteogenesis by performing JC-10 staining. After 3 days of NP exposure, no significant effects were observed. However, a non-significant depolarization was observed for all NP concentrations with respect to C+; this was most visible after 10 µg/ml AgNP exposure. Significant differences were observed after 7 days of NP exposure between the lowest and highest concentration for each NP type (fig 2). After 7 days of exposure to 10 µg/ml AgNPs significant polarization was observed compared to 1 µg/ml AgNPs, and compared to C+. The effects of TiO_2 and PSNPs were more in line with what was expected, results comparable to the C+. For both TiO_2 and PSNP exposure, it was observed that higher NP concentrations resulted in a lower 590/520 ratio after 7 days of exposure compared to C+. This indicated significantly more damage than the lower NP exposure after 7 days (fig 2).

Furthermore, after 7 days of osteogenesis induction, a significant depolarization was observed between C+ and CCCP compared to the C-. After 3 days, a non-significant depolarization was observed when comparing C+ and CCCP with C- (fig 2). Since this assay was optimized in a non-osteogenic setting, it explains why the effect of CCCP was not visible toward C+. Optimization in an osteogenic setting or performing another ROS assay to validate this data is suggested. During osteogenesis, the mitochondria provide the cell

with energy via oxidative phosphorylation (29). However, oxidative phosphorylation is also one of the main processes where ROS is produced (51-53), which could explain more depolarization in C+ compared to C-.

Mitochondrial morphological changes due to NP exposure – Mitochondria provides the cell with energy during osteogenesis, by the process of oxidative phosphorylation (29), which is linked with the fusion and the elongation of the organelle (31, 32). After 3 and 7 days of osteogenesis

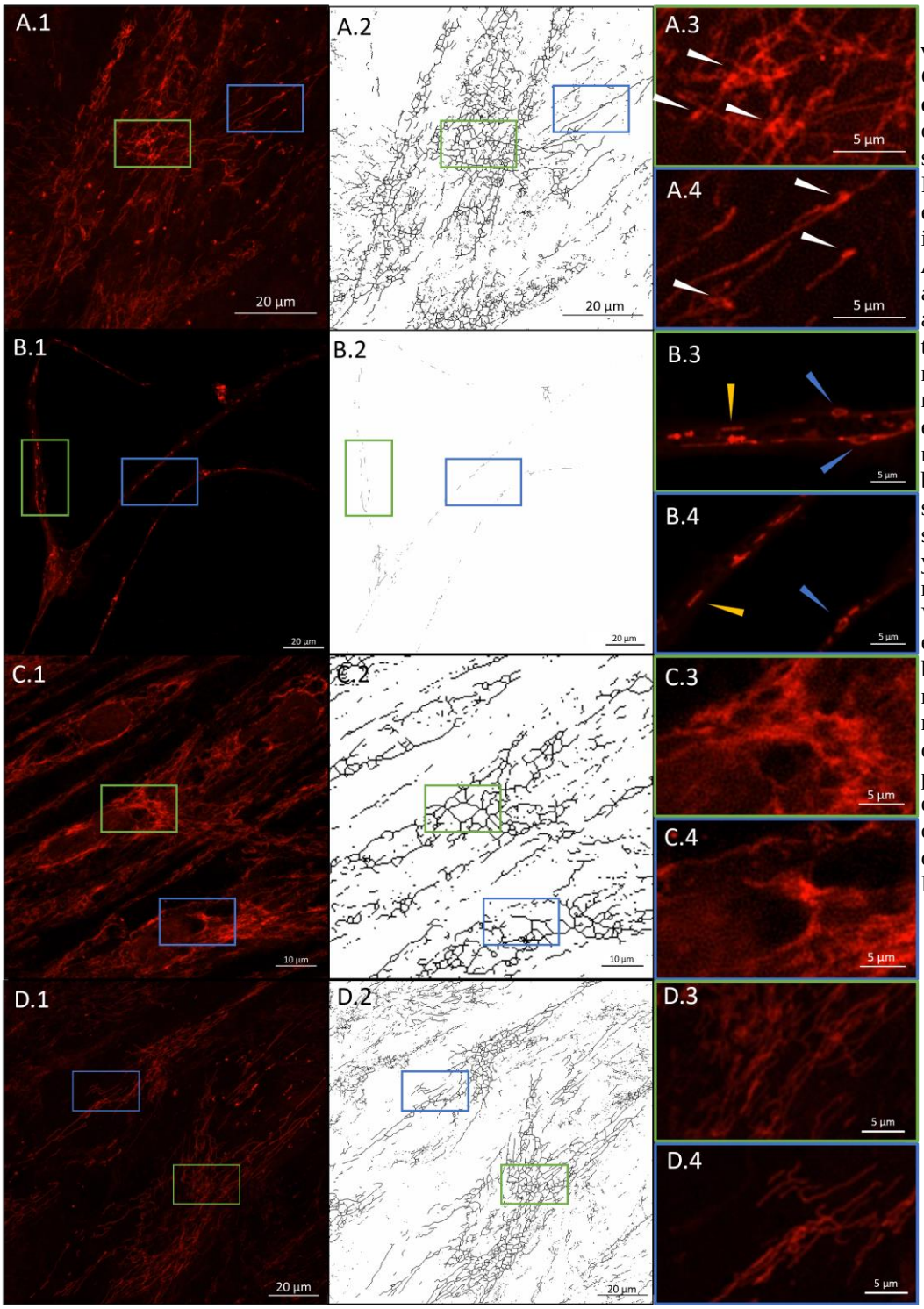

Figure 3 – Mitochondrial visualization with Mitotracker Red CMXRos after 7 days of NP exposure. Image A.1 - D.1 shows the overview picture. Image A.2 - D.2 are skeletonized images of A.1 – D.1. Images A.3 – D.3 and A.4 – D.4 3 are enlargement of the selected regions indicated with an green or blue border. **A**. Mitochondrial network of hDPSCs after 100 µg/ml PSNP exposure. White arrow indicate mitochondria thickening, which could suggest mitochondrial biogenesis. **B**. hDPSCs mitochondria after 10 µg/ml AgNP exposure. Degradation of mitochondria complex was observed by the punctate morphology and smaller fragments. Blue arrow indicate swollen punctuate mitochondria, and yellow arrow indicate short mitochondria fragments. **C**. Visualization of mitochondria after exposure of 100 µg/ml TiO_2NPs to hDPSCs. More dense mitochondria network is observed. **D**. hDPSCs mitochondria after 7 days of osteogenesis induction. Scale bars are present in the lower right corner of each figure. Images are taken with confocal microscopy with 40x water objective and laser 561 nm for MitoTracker Red CMXRos.

induction, mitochondria with a tubular-like morphology with a diameter of ~ 1 µm are observed (fig 3.D, S1.D, and S2.D). After 3 days of osteogenesis induction, swollen mitochondrial structures could be observed, which were most of the time present at the end of a mitochondrial elongation (fig S2.D3 and D4, white arrow). Since size and mass increase with mitochondrial biogenesis (54), this suggests that these structures (~ 1,25 µm) are newly formed mitochondria (fig S2.D3 and D4, white arrow).

TiO_2NP exposure resulted in tubular-like mitochondria that were more elongated, more branched, and denser network compared to C+ after 100 µg/ml TiO_2NP exposure after 3 days and 10 and 100 µg/ml after 7 days of TiO_2NP exposure (fig 3.C, fig S1.C, and S2.C). This implies that fusion processes and mitochondrial biogenesis are more pronounced after TiO_2NP exposure compared to C+. Zhoa H. et al. investigated the effect of TiO_2NP (Z-average of 270.73 ± 5.19 nm) exposure on the mitochondria and observed that after exposure, mitochondria appeared to punctate, which was linked to ROS production and mitochondrial imbalance (55). However, this study was not performed on differentiating cells. This could suggest that, in our case, in an osteogenesis setting, TiO_2NP exposure could improve the activation of the fusion process.

Cells' exposure to PSNPs showed mitochondrial morphologies similarities to C+. Both after 10 and 100 µm/ml of PSNP exposure for 3 and 7 days, mitochondria were present as long tubular-like structures similar to the C+ samples (fig 3.A, S1.A, and S2.A). These results indicate that PSNPs had almost no effect on mitochondrial functioning. However, after 7 days of 10 µg/ml PSNP exposure, round swollen structures with a diameter of ~1.5 µm, which is larger than the normal average diameter of 1 µm (fig S2.A4), were present. These structures are different from the punctuate morphology that was observed after AgNP exposure, and fluorescence intensity is also weaker compared to that of the swollen mitochondria after AgNP exposure (fig S1.A). Here, mitochondria biogenesis could be visible through their abundant presence around the nucleus (fig S1.A) (56, 57).

In a normal situation, elongated mitochondria are observed, such as in C+, since this is the normal morphology of mitochondria in MSCs (29). However, after AgNP exposure, small punctate mitochondria, together with the fragmentation of the mitochondrial network, are observed (fig 4.C, S1.C, and S2.C, blue and yellow arrow). This was observed for all three tested conditions of AgNP exposure, but these observations were more pronounced after 10 µg/ml AgNP exposure for 3 and 7 days (fig 3.C and S2.C). The same effect was observed by Li J. et al., who investigated the effect of AgNP exposure on the HepG2 cell line. Fission processes were observed where a punctuated morphology and shorter fragments of mitochondria were noticed after AgNP exposure (58). Long and branched mitochondria are characterized by fusion, which happens during differentiation. While fission is linked with proliferation, this suggests that during AgNP exposure, the cells and their organelles undergo oxidative stress and damage. This could lead to cell death, which was also observed during the ARS assay. Since the normal morphology of mitochondrial network in MSCs is an elongated tubular morphology, this suggests that AgNP exposure resulted in ROS production and oxidative stress, which could result in degradation and smaller fragments of the mitochondrial network. However, further research is needed to confirm this statement. ROS measurements like H_2O_2 and Amplex Red assay, live imaging of mitochondria, which could show how mitochondrial morphology changed through time after NP exposure, and gene expression are recommended.

Osteogenesis- and mitochondria-related genes underlying the regulation of osteogenesis – A literature study was performed on selected genes that play a role in the regulation of osteogenesis and how this regulation could be influenced by NP exposure (table S1). A summary of the literature study is presented in fig 4. In a normal situation (without NP exposure), the activation of the Wnt/β-catenin pathway happens by the binding of Wnt proteins (Wnt3a and Wnt5a) to Frizzled receptor (59, 60). Activation of the pathway enables the formation and accumulation of β-catenin in the cytoplasm, which will be translocated to the nucleus, where it will bind to the transcription factor of RUNX2 (60, 61). RUNX2 is the master regulator of osteogenesis. When this protein is transcribed, the activation of osteogenesis occurs (34, 35). Consequently, RUNX2 drives the transcription of several osteogenesis genes. At first,

SP7 will become expressed, which causes the transcription of the bone mineralization genes COL1A1, ALP, OPN, and OCN (62, 63). Mitochondria provide the cell with energy through oxidative phosphorylation, which can be activated by Wnt3a (29, 64). During this process of oxidative phosphorylation, Acetyl-CoA is formed, binding this molecule to β-catenin, which causes the activation of β-catenin and prevents this molecule from degrading (30). The upregulation of mitochondrial fusion genes (OPA1, MNF1, and MNF2) is observed during osteogenesis (65). The expression of these genes is linked to mitochondrial biogenesis, mitochondria elongation and oxidative phosphorylation (66, 67). Further, the expression of OPA1 results in elongation, and an increase in cristae in the inner mitochondrial membrane (66, 67). Overall, these processes of mitochondrial fusion could support energy production to fulfill the energy need for the mitochondrial biogenesis during osteogenesis, for example.

However, exposure to different NPs can influence the regulation. AgNPs (indicated as dark blue NPs) can release Ag^+-ions. These molecules are reactive toward biological structures such as the mitochondria (58, 68). This interaction could cause the formation of ROS (58, 69). It is known that the presence of ROS could inhibit osteogenesis and promote adipogenesis(20, 23). The presence of ROS further inhibits the fusion processes and activates the fission processes of the mitochondria, since higher levels of cell stress are linked to fission (70). Here it is expected that AgNP exposure inhibits the expression of osteogenesis-related genes. Through the inert properties of TiO_2NPs, the formation of adverse effects, such as ROS, is minor. This is why it is expected that exposure to TiO_2NPs (light blue NPs will not negatively affect osteogenesis (13) (fig 5). However, different studies showed an upregulation of the osteogenesis genes after TiO_2NP exposure (71, 72). However, other studies observed that TiO_2NP exposure resulted in a decrease in osteogenesis-related genes (73). Our data showed a significant increase in calcium formation after TiO_2NP exposure (fig 1B). Mitochondrial morphology showed mitochondrial fusion processes, where elongation of the mitochondria was even more pronounced than in C+ (fig 3, S1, S2). This suggests that TiO_2NP exposure induces osteogenesis by an interaction between mitochondrial- and osteogenesis-related genes. Because the biocompatible characteristics of the PSNPs (orange NPs), it is not expected that exposure to PSNPs will show a negative effect on osteogenesis capacity and on mitochondrial parameters (20). Ren L. et al. observed an upregulation of mitochondrial fusion genes and a downregulation of fission genes after PSNP exposure (74). Here, we expect that PSNP exposure results in an upregulation of both osteogeneses- and mitochondrial-related genes, which will result in an increase in osteogenesis.

Designed primers did not fulfill efficiency criteria for gene expression on exposed hDPSCs in the osteogenesis context – Based on the literature, osteogenesis genes were selected, and primers were designed using Primer3. Primers were tested on mixed samples of differentiated hDPSCs exposed to NPs, and efficiency was determined. Primers were designed with 100 % coverage and to target the target gene. However, many of the primers did not bind or were not specific enough (table S1). Several factors could cause this outcome.

A higher input concentration might be needed, although the usual input concentration (5-20 ng/µl) was well within the range of the tested dilution series (28 – 0,4375 ng/µl). Amplification of the tested genes was not detectable, possibly through low gene expression levels after the selected time points.

Another problem could be the Tm; this should be between 57 – 63 °C, although, after manufacturing the primers, the Tm changed from the expected Tm as indicated on Primer3. Designed primers had a Tm between 50 – 58 °C, which is, in most cases, below the minimum Tm of 57 °C. Also, the maximum differences in Tm between the reversed and forward primer should be 1 °C. However, this was mainly more than the maximum that was set. The effect on the gene expression of a too low Tm results that primers could bind with sequences other than the target sequence. Which results in a non-specific PCR-amplification and not enough yield (75). In this case, redesigning the primers could be a solution.

Primers were designed with a set of parameters. One parameter that was not considered was to design them to span two exons, which should result in more specific binding and prevent amplification of (g)DNA contamination. In this case, the cDNA was treated with gDNA wipeout;

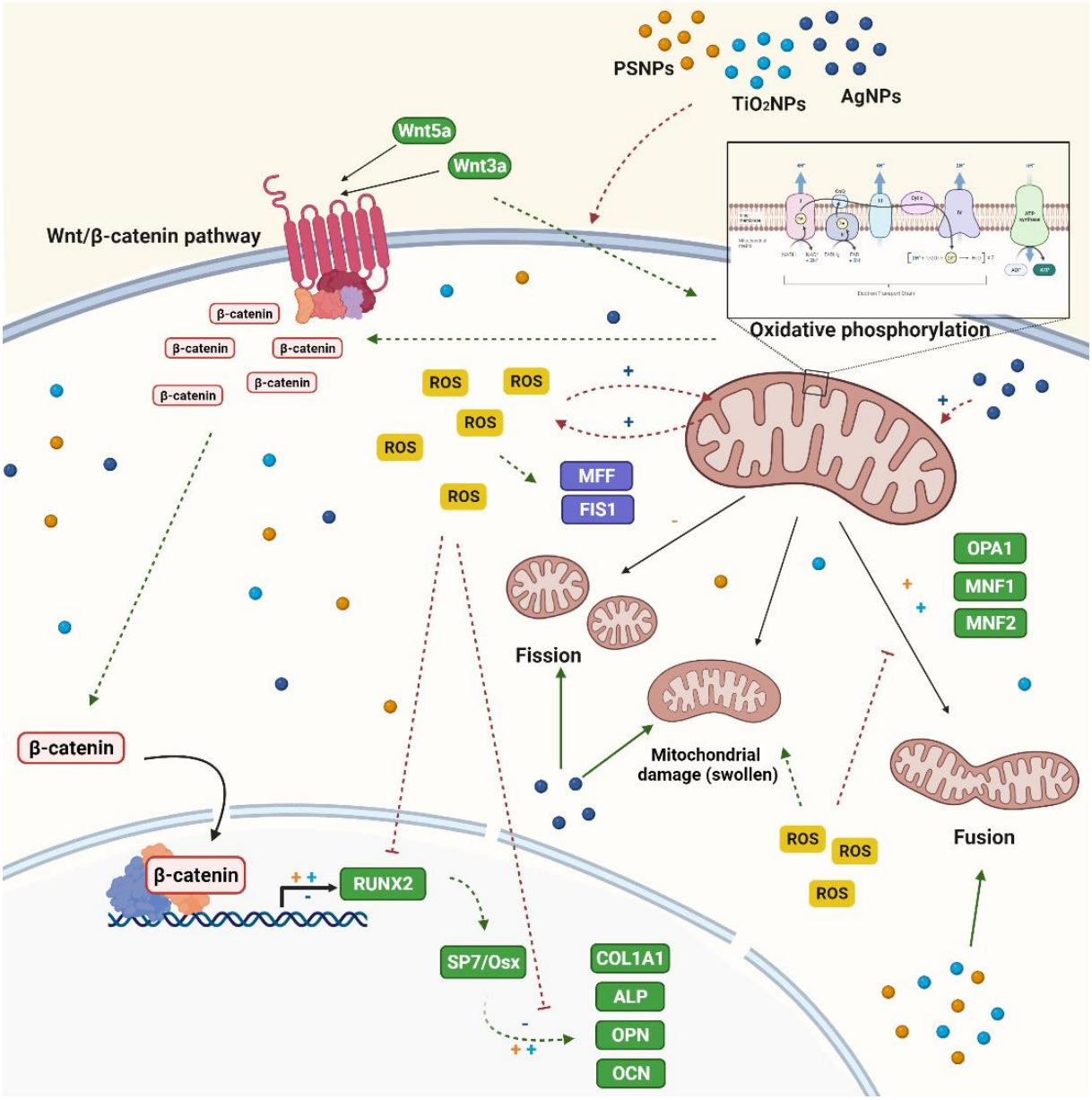

Figure 4 – Summary of the different players during osteogenesis: Binding of WNT Family Member3A and 5A (WNT3A and WNT5A) to the Frizzled receptor results in activating of the Wnt/β-catenin pathway, which results in the formation and accumulation of β-catenin in the cytoplasm. β-catenin will be translocated to the nucleus, where it will bind to the transcription factor Runt-related transcription factor 2 (*RUNX2),* resulting in transcription of RUNX2. RUNX2 will cause the transcription of Osterix (SP7/Osx), followed by the other osteogenesis-related genes, namely: Collagen type I alpha (COL1A1), Alkaline Phosphatase (ALP), Osteopontin (OPN), and Osteocalcin (OCN). Furthermore, the interaction of the mitochondria plays an important role. The presence of WNT3A can increase oxidative phosphorylation, which is the main mechanism of energy production during osteogenesis. During oxidative phosphorylation, Acetyl-CoA is formed, which causes the activation of β-catenin. Further, the upregulation of different fusion genes, Mitofusion 1 and 2 (MNF1 and MNF2), and OPA1 Mitochondrial Dynamin Like GTPase (OPA1), Mitochondrial fission protein 1 and 2 (FIS1 and FIS2), is linked with the osteogenesis processes and a decrease in fission related genes (Mitochondrial Fission Factor (MFF) Mitochondrial fission protein 1 (FIS1)). The influence of nanoparticle (NP) exposure can have different results. Silver NPs (AgNPs) can release Ag^{+}-ions, which can interact with the mitochondria, resulting in ROS formation. This ROS could lead to oxidative stress, damage to the mitochondria, and inhibition of the expression of fusion and osteogenesis-related genes. Exposure to titanium dioxide (TiO_2) and polystyrene (PS)NPs results in upregulation of both the mitochondrial fusion and osteogenesis related genes. Own observations are indicated with a full line, while findings out literature are indicated with a dashed line. Image created with BioRender.

the chance that the sample was still contaminated with gDNA was minor.

However, another challenge in primer testing could be our samples themselves. In this experiment, different samples are used, all in different stages of osteogenesis. After 3,7, and 14 days of osteogenesis induction, samples are harvested for gene expression. Different gene expression levels of the different genes are expected over time by performing gene expression at different stages of osteogenesis. Primers were first tested on a mixed sample from the different conditions, where only six primers were efficient. However, amplification of the genes could have taken place for some conditions but might have been undetectable through a dilution effect when measuring in a mixed sample of conditions. Further, NP remnants in the cDNA samples could be present, which could interfere with the qPCR reaction and result in less amplification. This could be observed in a lower cycle threshold (CT) value and a lower amplification curve. Furthermore, the mixed sample, which contained multiple conditions of NPs concentrations, makes it challenging to interpret the obtained results since different NPs and conditions could cause different expression levels. So testing of the primers should be performed on individual samples to know how NPs will interact with the gene expression and which NPs will result in an up- or downregulation of the specific genes through time. Further, RT-qPCR products could be evaluated with gel electrophoresis to study if the reaction was successful.

Four primers (RUNX2, ALP, OCN, and COL1A1) were tested a second time only on C+ samples of 7 and 14 days because it was expected that at these time points, the selected genes came to expression and to remove possible NP interference. However, after this second trial, only COL1A1 came to expression. This indicates that the lack of amplification after qPCR was due to variance in samples and the designed primers, as mentioned before.

CONCLUSION

This study investigated the effect of three commonly used NPs (Ag, TiO_2, and PSNPs) on the mitochondrial functioning, which could affect the differentiation capacity of hDPSCs. Cells were exposed to different concentrations of Ag, TiO_2, and PSNPs for 3, 7, and or 14 days. Exposure to PSNPs showed that PSNPs did not affect the calcium formation during osteogenesis. Mitochondrial membrane potential showed a non-significant depolarization with higher PSNP exposure after 7 days, which suggests that PSNPs could induce ROS formation and affect mitochondrial membrane potential. Furthermore, similar mitochondrial morphology was observed compared to C+.

First results of TiO_2NP exposure resulted in a significant increase in calcium formation, with higher NP concentrations. However, it was observed that longer exposure to higher TiO_2NP concentrations was linked with cell death. Imaging of mitochondria showed a more dense mitochondrial network, more branching, and more elongated mitochondria compared to C+, which could indicate that TiO_2NPs promote mitochondria fusion and biogenesis. At the same time, mitochondrial membrane potential showed depolarization after exposure to 100 µg/ml TiO_2NP for 7 days compared to 3 days.

A decrease in calcium formation and an increase in cell death were observed after AgNP exposure. However, stained calcium nodules were observed after 14 days of 1 µg/ml AgNP exposure. A decline in the 520/590 ratio was noticed after AgNP exposure. Morphology of the mitochondria was significantly affected by AgNP exposure. However, after 10 µg/ml AgNP exposure for 7 days a more pronounced polarization was present. The exposure caused fragmentation of mitochondrial network and punctuated morphology of individual mitochondria. These results indicate that AgNP exposure results in ROS formation and oxidative stress, which could inhibit the different interplays during osteogenesis.

Furthermore, it was noticed that cell passage could influence osteogenesis. Older cell passages showed fewer cells, but these were more differentiated. While in the younger cell passage, more cells were observed but less differentiation. This could mean that older cells lose some of the proliferation capacity due to NP exposure or shift their energy production towards differentiation only instead of both developmental processes. These results implicate that this research's hypothesis is accepted; exposure to AgNP in hDPSC will result in mitochondrial dysfunction,

possibly due to oxidative stress, leading to alterations in the osteogenic capacity of hDPSC.

Furthermore, exposure to TiO_2 and PSNPs, could promote mitochondrial functioning and osteogenesis. However, gene expression should be conducted to get more clarity regarding the different osteogenesis, mitochondrial, and oxidative stress factors, together with another validation test of osteoblast formation and ROS assays. More upstream studies could provide crucial information about the effects of NP exposure in the early stages of development. Furthermore, interpretation of the results suggests that mitochondrial parameters could be used for biomarker development and risk assessment strategies.

REFERENCES

1. Missaoui WN, Arnold RD, Cummings BS. Toxicological status of nanoparticles: What we know and what we don't know. Chem Biol Interact. 2018;295:1-12.
2. Blaznik U, Krušič S, Hribar M, Kušar A, Žmitek K, Pravst I. Use of Food Additive Titanium Dioxide (E171) before the Introduction of Regulatory Restrictions Due to Concern for Genotoxicity. Foods. 2021;10(8):1910.
3. Zhang X-F, Liu Z-G, Shen W, Gurunathan S. Silver Nanoparticles: Synthesis, Characterization, Properties, Applications, and Therapeutic Approaches. International journal of molecular sciences. 2016;17(9):1534.
4. Simko M, Fiedeler U, Gazsó A, Nentwich M. How Nanoparticles Enter the Human Body and Their Effects There. http://hwoeawacat/nanotrust-dossier. 2011.
5. Ding DC, Shyu WC, Lin SZ, Li H. Current concepts in adult stem cell therapy for stroke. Curr Med Chem. 2006;13(29):3565-74.
6. Ding DC, Shyu WC, Lin SZ, Li H. The role of endothelial progenitor cells in ischemic cerebral and heart diseases. Cell Transplant. 2007;16(3):273-84.
7. Ding DC, Shyu WC, Lin SZ. Mesenchymal stem cells. Cell Transplant. 2011;20(1):5-14.
8. Hanna H, Mir LM, Andre FM. In vitro osteoblastic differentiation of mesenchymal stem cells generates cell layers with distinct properties. Stem Cell Research & Therapy. 2018;9(1):203.
9. Klaine SJ, Koelmans AA, Horne N, Carley S, Handy RD, Kapustka L, et al. Paradigms to assess the environmental impact of manufactured nanomaterials. Environmental Toxicology and Chemistry. 2012;31(1):3-14.
10. Zhang L, Gu FX, Chan JM, Wang AZ, Langer RS, Farokhzad OC. Nanoparticles in medicine: therapeutic applications and developments. Clin Pharmacol Ther. 2008;83(5):761-9.
11. Najahi-Missaoui W, Arnold RD, Cummings BS. Safe Nanoparticles: Are We There Yet? International journal of molecular sciences. 2020;22(1):385.
12. Trivedi MK, Murase J. Titanium Dioxide in Sunscreen. 2017.
13. Skocaj M, Filipic M, Petkovic J, Novak S. Titanium dioxide in our everyday life; is it safe? Radiol Oncol. 2011;45(4):227-47.
14. Stensberg MC, Wei Q, McLamore ES, Porterfield DM, Wei A, Sepúlveda MS. Toxicological studies on silver nanoparticles: challenges and opportunities in assessment, monitoring and imaging. Nanomedicine (Lond). 2011;6(5):879-98.
15. Shah AA, Hasan F, Hameed A, Ahmed S. Biological degradation of plastics: A comprehensive review. Biotechnology Advances. 2008;26(3):246-65.
16. Wegner A, Besseling E, Foekema EM, Kamermans P, Koelmans AA. Effects of nanopolystyrene on the feeding behavior of the blue mussel (Mytilus edulis L.). Environ Toxicol Chem. 2012;31(11):2490-7.
17. Imhof HK, Schmid J, Niessner R, Ivleva NP, Laforsch C. A novel, highly efficient method for the separation and quantification of plastic particles in sediments of aquatic environments. Limnology and Oceanography: Methods. 2012;10(7):524-37.
18. Nowack B, Bucheli TD. Occurrence, behavior and effects of nanoparticles in the environment. Environ Pollut. 2007;150(1):5-22.
19. Zhu H, Han J, Xiao JQ, Jin Y. Uptake, translocation, and accumulation of manufactured iron oxide nanoparticles by pumpkin plants. J Environ Monit. 2008;10(6):713-7.
20. Loos C, Syrovets T, Musyanovych A, Mailänder V, Landfester K, Nienhaus GU, et al. Functionalized polystyrene nanoparticles as a platform for studying bio–nano interactions. Beilstein Journal of Nanotechnology. 2014;5:2403-12.
21. Kik K, Bukowska B, Sicińska P. Polystyrene nanoparticles: Sources, occurrence in the environment, distribution in tissues, accumulation and toxicity to various organisms. Environmental Pollution. 2020;262:114297.

22. Brown DM, Wilson MR, MacNee W, Stone V, Donaldson K. Size-Dependent Proinflammatory Effects of Ultrafine Polystyrene Particles: A Role for Surface Area and Oxidative Stress in the Enhanced Activity of Ultrafines. Toxicology and Applied Pharmacology. 2001;175(3):191-9.
23. He W, Elkhooly TA, Liu X, Cavallaro A, Taheri S, Vasilev K, et al. Silver nanoparticle based coatings enhance adipogenesis compared to osteogenesis in human mesenchymal stem cells through oxidative stress. Journal of Materials Chemistry B. 2016;4(8):1466-79.
24. Atashi F, Modarressi A, Pepper MS. The role of reactive oxygen species in mesenchymal stem cell adipogenic and osteogenic differentiation: a review. Stem Cells Dev. 2015;24(10):1150-63.
25. Jamieson DJ. Oxidative stress responses of the yeast Saccharomyces cerevisiae. Yeast. 1998;14(16):1511-27.
26. Finkel T. Signal transduction by reactive oxygen species. J Cell Biol. 2011;194(1):7-15.
27. Manivannan A, Soundararajan P, Jeong BR. Role of Reactive Oxygen Species Signaling in Cell Proliferation and Differentiation. Reactive Oxygen Species in Plants2017. p. 319-29.
28. Li J, Chen Y, Yang Y, Kawazoe N, Chen G. Sub-10 nm gold nanoparticles promote adipogenesis and inhibit osteogenesis of mesenchymal stem cells. Journal of Materials Chemistry B. 2017;5(7):1353-62.
29. Chen CT, Shih YR, Kuo TK, Lee OK, Wei YH. Coordinated changes of mitochondrial biogenesis and antioxidant enzymes during osteogenic differentiation of human mesenchymal stem cells. Stem Cells. 2008;26(4):960-8.
30. Shares BH, Busch M, White N, Shum L, Eliseev RA. Active mitochondria support osteogenic differentiation by stimulating β-catenin acetylation. Journal of Biological Chemistry. 2018;293(41):16019-27.
31. Li Q, Gao Z, Chen Y, Guan M-X. The role of mitochondria in osteogenic, adipogenic and chondrogenic differentiation of mesenchymal stem cells. Protein Cell. 2017;8(6):439-45.
32. Forni MF, Peloggia J, Trudeau K, Shirihai O, Kowaltowski AJ. Murine Mesenchymal Stem Cell Commitment to Differentiation Is Regulated by Mitochondrial Dynamics. Stem Cells. 2016;34(3):743-55.
33. Spurlock B, Tullet JMA, Hartman JL, Mitra K. Interplay of mitochondrial fission-fusion with cell cycle regulation: Possible impacts on stem cell and organismal aging. Experimental Gerontology. 2020;135:110919.
34. Rutkovskiy A, Stensløkken K-O, Vaage IJ. Osteoblast Differentiation at a Glance. Med Sci Monit Basic Res. 2016;22:95-106.
35. Han N, Zheng Y, Li R, Li X, Zhou M, Niu Y, et al. β-catenin enhances odontoblastic differentiation of dental pulp cells through activation of Runx2. PLoS One. 2014;9(2):e88890-e.
36. Guildford AL, Poletti T, Osbourne LH, Di Cerbo A, Gatti AM, Santin M. Nanoparticles of a different source induce different patterns of activation in key biochemical and cellular components of the host response. J R Soc Interface. 2009;6(41):1213-21.
37. Valente AJ, Maddalena LA, Robb EL, Moradi F, Stuart JA. A simple ImageJ macro tool for analyzing mitochondrial network morphology in mammalian cell culture. Acta Histochemica. 2017;119(3):315-26.
38. Bhattacharjee S. DLS and zeta potential - What they are and what they are not? J Control Release. 2016;235:337-51.
39. Nguyen VH, Lee B-J. Protein corona: a new approach for nanomedicine design. International journal of nanomedicine. 2017;12:3137-51.
40. Patel VR, Agrawal YK. Nanosuspension: An approach to enhance solubility of drugs. J Adv Pharm Technol Res. 2011;2(2):81-7.
41. Mudalige T, Qu H, Van Haute D, Ansar SM, Paredes A, Ingle T. Chapter 11 - Characterization of Nanomaterials: Tools and Challenges. In: López Rubio A, Fabra Rovira MJ, martínez Sanz M, Gómez-Mascaraque LG, editors. Nanomaterials for Food Applications: Elsevier; 2019. p. 313-53.
42. Ren Y, Feng X, Lang X, Wang J, Du Z, Niu X. Evaluation of Osteogenic Potentials of Titanium Dioxide Nanoparticles with Different Sizes and Shapes. Journal of Nanomaterials. 2020;2020:1-13.

43. Hou Y, Cai K, Li J, Chen X, Lai M, Hu Y, et al. Effects of titanium nanoparticles on adhesion, migration, proliferation, and differentiation of mesenchymal stem cells. International journal of nanomedicine. 2013;8:3619-30.
44. Kurepa J, Paunesku T, Vogt S, Arora H, Rabatic BM, Lu J, et al. Uptake and distribution of ultrasmall anatase TiO2 Alizarin red S nanoconjugates in Arabidopsis thaliana. Nano Lett. 2010;10(7):2296-302.
45. Thurn KT, Paunesku T, Wu A, Brown EMB, Lai B, Vogt S, et al. Labeling TiO2 nanoparticles with dyes for optical fluorescence microscopy and determination of TiO2-DNA nanoconjugate stability. Small. 2009;5(11):1318-25.
46. Puchtler H, Meloan SN, Terry MS. On the history and mechanism of alizarin and alizarin red S stains for calcium. J Histochem Cytochem. 1969;17(2):110-24.
47. He W, Zheng Y, Feng Q, Elkhooly TA, Liu X, Yang X, et al. Silver nanoparticles stimulate osteogenesis of human mesenchymal stem cells through activation of autophagy. Nanomedicine (Lond). 2020;15(4):337-53.
48. Zhang R, Lee P, Lui VCH, Chen Y, Liu X, Lok CN, et al. Silver nanoparticles promote osteogenesis of mesenchymal stem cells and improve bone fracture healing in osteogenesis mechanism mouse model. Nanomedicine: Nanotechnology, Biology and Medicine. 2015;11(8):1949-59.
49. Martin-Piedra MA, Garzon I, Oliveira AC, Alfonso-Rodriguez CA, Sanchez-Quevedo MC, Campos A, et al. Average cell viability levels of human dental pulp stem cells: an accurate combinatorial index for quality control in tissue engineering. Cytotherapy. 2013;15(4):507-18.
50. Martin-Piedra MA, Garzon I, Oliveira AC, Alfonso-Rodriguez CA, Carriel V, Scionti G, et al. Cell viability and proliferation capability of long-term human dental pulp stem cell cultures. Cytotherapy. 2014;16(2):266-77.
51. Madamanchi NR, Runge MS. Mitochondrial Dysfunction in Atherosclerosis. Circulation Research. 2007;100(4):460-73.
52. Thomas SR, Witting PK, Drummond GR. Redox control of endothelial function and dysfunction: molecular mechanisms and therapeutic opportunities. Antioxid Redox Signal. 2008;10(10):1713-65.
53. Li X, Fang P, Mai J, Choi ET, Wang H, Yang X-f. Targeting mitochondrial reactive oxygen species as novel therapy for inflammatory diseases and cancers. Journal of hematology & oncology. 2013;6:19-.
54. Bhatti JS, Kumar S, Vijayan M, Bhatti GK, Reddy PH. Chapter Two - Therapeutic Strategies for Mitochondrial Dysfunction and Oxidative Stress in Age-Related Metabolic Disorders. In: Reddy PH, editor. Progress in Molecular Biology and Translational Science. 146: Academic Press; 2017. p. 13-46.
55. Zhao H, Chen L, Zhong G, Huang Y, Zhang X, Chu C, et al. Titanium Dioxide Nanoparticles Induce Mitochondrial Dynamic Imbalance and Damage in HT22 Cells. Journal of Nanomaterials. 2019;2019:4607531.
56. Hofmann AD, Beyer M, Krause-Buchholz U, Wobus M, Bornhäuser M, Rödel G. OXPHOS supercomplexes as a hallmark of the mitochondrial phenotype of adipogenic differentiated human MSCs. PLoS One. 2012;7(4):e35160-e.
57. Quinn KP, Sridharan GV, Hayden RS, Kaplan DL, Lee K, Georgakoudi I. Quantitative metabolic imaging using endogenous fluorescence to detect stem cell differentiation. Scientific reports. 2013;3:3432-.
58. Li J, Zhang B, Chang X, Gan J, Li W, Niu S, et al. Silver nanoparticles modulate mitochondrial dynamics and biogenesis in HepG2 cells. Environmental Pollution. 2020;256:113430.
59. Okamoto M, Udagawa N, Uehara S, Maeda K, Yamashita T, Nakamichi Y, et al. Noncanonical Wnt5a enhances Wnt/β-catenin signaling during osteoblastogenesis. Scientific Reports. 2014;4(1):4493.
60. Katoh M, Katoh M. Comparative genomics on Wnt8a and Wnt8b genes. Int J Oncol. 2005;26(4):1129-33.
61. Komori T. Signaling networks in RUNX2-dependent bone development. Journal of Cellular Biochemistry. 2011;112(3):750-5.

62. Nakashima K, Zhou X, Kunkel G, Zhang Z, Deng JM, Behringer RR, et al. The novel zinc finger-containing transcription factor osterix is required for osteoblast differentiation and bone formation. Cell. 2002;108(1):17-29.
63. Kirkham G, Cartmell S. Genes and Proteins Involved in the Regulation of Osteogenesis. Topics in Tissue Engineering. 2007;3.
64. Smith CO, Eliseev RA. Energy Metabolism During Osteogenic Differentiation: The Role of Akt. Stem cells and development. 2021;30(3):149-62.
65. Hall AR, Burke N, Dongworth RK, Hausenloy DJ. Mitochondrial fusion and fission proteins: novel therapeutic targets for combating cardiovascular disease. Br J Pharmacol. 2014;171(8):1890-906.
66. Cipolat S, Brito OMd, Zilio BD, Scorrano L. OPA1 requires mitofusin 1 to promote mitochondrial fusion. Proceedings of the National Academy of Sciences. 2004;101(45):15927-32.
67. Carmona-Carmona CA, Dalla Pozza E, Ambrosini G, Errico A, Dando I. Divergent Roles of Mitochondria Dynamics in Pancreatic Ductal Adenocarcinoma. Cancers (Basel). 2022;14(9).
68. Yuan L, Gao T, He H, Jiang FL, Liu Y. Silver ion-induced mitochondrial dysfunction via a nonspecific pathway. Toxicol Res (Camb). 2017;6(5):621-30.
69. Bressan E, Ferroni L, Gardin C, Rigo C, Stocchero M, Vindigni V, et al. Silver nanoparticles and mitochondrial interaction. Int J Dent. 2013;2013:312747-.
70. Youle RJ, van der Bliek AM. Mitochondrial fission, fusion, and stress. Science. 2012;337(6098):1062-5.
71. Chuang Y-C, Chang C-C, Yang F, Simon M, Rafailovich M. TiO2 nanoparticles synergize with substrate mechanics to improve dental pulp stem cells proliferation and differentiation. Materials Science and Engineering: C. 2021;118:111366.
72. Wang Y, Jiang Z, Yu K, Feng Y, Xi Y, Lai K, et al. Improved osseointegrating functionality of cell sheets on anatase TiO 2 nanoparticle surfaces. RSC Adv. 2017;7:35845-53.
73. Hu H, Chen L, Li ST, Pan QY, Liu YP. Nano-TiO2 particles inhibit the biological behavior and mineralization of bone marrow mesenchymal stem cells transfected with CXCR4. Eur Rev Med Pharmacol Sci. 2021;25(1):71-7.
74. Ren L, Chen X, Chen X, Li J, Cheng B, Xia J. Mitochondrial Dynamics: Fission and Fusion in Fate Determination of Mesenchymal Stem Cells. Frontiers in Cell and Developmental Biology. 2020;8.
75. Rychlik W, Spencer WJ, Rhoads RE. Optimization of the annealing temperature for DNA amplification in vitro. Nucleic Acids Res. 1990;18(21):6409-12.

Acknowledgements – First of all, I would like to thank my two PI's, prof. dr. Karen Smeets and dr. Nelly Saenen, for making it possible to perform my senior internship at this research institute and for the guidance I received during my internship. Secondly, and most importantly, my most enormous thanks go to my supervisor Margo Witters for all the time she took to explain and teach me everything, and to guide me through this whole process. She let me see I was able to work independently and allowed me to imply my own interests in this research, and to let me see it was ok to make mistakes. Next, I want to thank dr. Vincent Jeanen for all the help he provided me with and for analyzing the samples under confocal microscopy. Further, I want to thank Buse Turkeli and Britt Bemelmans, for all the help I received from them in the lab during my thesis and for being there when I had a difficult time. Also, my friends, Annelore B., Anne S., Margo S., and Marie-Lien VD. for all the support that I received these last months. My sister and boyfriend who saw me at my worst and did everything to bring back the peace in my head. My dog Bambi, who was always ready for a walk during my breaks. At last, I wanted to thank my parents for the belief they had in me when I started this journey five years ago and provided me with everything they could to make sure that I could complete this journey.

Author contributions – Prof. dr. Smeets Karen and dr. Saenen Nelly conceived and designed the research. Experiments and data analysis were performed by Browko Ellen. Dr. Jeanen Vincent analyzed the samples from the MitoTracker assay with confocal microscopy. Browko Ellen wrote the paper, and was reviewed by Witters Margo. All authors carefully edited the manuscript

SUPPLEMENT

Sample collection, RNA extraction and cDNA synthesis

To study the effects of NPs on gene expression of the selected genes, 1 x 10^4 cells were seeded in a 24 - well plate and were differentiated for 3, 7, and 14 days with or without a NP exposure. These conditions were: C+, C-, 1 and 10 µg/ml AgNPs, and 10 and 100 µg/ml TiO_2 and PSNPs. Cells were collected according to the splitting protocol and the collected pellets were snap-frozen in liquid nitrogen and stored at -80 °C until extraction. The purity of the samples was checked using Nanodrop™ ND-1000 spectrophotometer (Thermo Fisher Scientific), where 260/280 ratio (~2.0) and 260/230 ration (~2.0 – 2.2) was checked. Samples were processed with a TURBO DNA-*free*™ kit (Thermo Fisher Scientific) to remove potential remaining genomic DNA (gDNA). Reverse transcriptase by using SuperScript™ III First-Strand synthesis Supermix kit (Invitrogen, Thermofisher Scientific) was used following manufacturer's instructions, to obtain complementary DNA (cDNA) with an output of ~ 1500 ng/µl cDNA. The final cDNA samples are stored at -20 °C.

Table S1: Forward and reversed sequences of the designed primers for osteogenesis, mitochondria and oxidative related genes and references genes. That are manufactured by Biolegio. Efficiency was tested and, efficiency of primers that were indicated as useful are indicated in ( ). Runt-related transcription factor 2 (RUNX2), Osteocalcin (OCN), Alkaline Phosphatase (ALP), Osteopontin (OPN), Collagen type I alpha (COL1A1), Osterix (Sp7), β-catenin, WNT Family Member3A and 5A (WNT3A and WNT5A), Mitofusion 1 (MNF1) Mitochondrial Fission Factor (MFF), OPA1 Mitochondrial Dynamin Like GTPase (OPA1), Mitochondrial fission protein 1 (FIS1), heat shock protein 10 (HSP10), Tumor protein P53 (P53), Glutathione peroxidase 4 (GPX4), Glutathione peroxidase 1 (GPX1), Glutathione-disulfide reductase (GSR), Catalase (CAT), Superoxide dismutase 1 (SOD1), TATA-Box Binding Protein (TBP), Glucuronidase Beta (GUSB), Succinate dehydrogenase complex, subunit A, flavoprotein variant (SDHA), Glyceraldehyde-3-Phosphate Dehydrogenase (GAPDH), Ribosomal Protein S18 (RPS18), Delta-aminolevulinate synthase 1 (ALAS1), Ribosomal protein L9 (RPL9), Actin Beta (ACTB), Beta2-microglobine (B2M), Ribosomal Protein Lateral Stalk Subunit P0 (RPLP0), and Ubiquitin C (UBC).

	Name gene	Reversed primer	Forwards primer	Efficiency
Osteogenesis related genes	RUNX2	TTCTCCAACCCACGAATGCA	GGTGTGGTAGTGAGTGGTGG	1,20E+24 %
	OCN	GTGCAGCCTTTGTGTCCAAG	GCCATTGATACAGGTAGCGC	276,39 %
	ALP	CGGAACTCCTGACCCTTGAC	TCCGTCACGTTGTTCCTGTT	-99,88 %
	OPN	GCCGAGGTGATAGTGTGGTT	AACGGGGATGGCCTTGTAT	Undetermined
	COL1A1	AAGACGAAGACATCCCACCAAC	AGATCACGTCATCGCACAAC	104,91 %
	SP7	GGCACAAAGAAGCCGTACTC	CACTGGGCAGACAGTCAGAA	Undetermined
	B-catenin	GGCTACTCAAGCTGATTTGATGG	CCAGTGACTAACAGCCGCTT	91,37 %
	WNT3a	CTTTGCAGTGACACGCTCAT	ACCATCCCACCAAACTCGAT	Undetermined
	WNT5a	ATTCACAGGTTCTCAGCCCA	TCACATCACAACACGGAGGA	Undetermined
Mitochondrial related genes	MFN1	CCTTTTACCTCAGCCTCCCA	CAGACCCAAGGATCCACACT	Undetermined
	MFF	AACCCCTGGCACTGAAAACA	TGAGGGGTTGTAGGAGGTCT	104,19 %
	OPA1	TCGGACCCAAGAACAGTGTG	GGTTCTTCCGGACTGTGGTT	7,4E+08 %
	FIS1	AGGCCTTAAAGTACGTCCGC	TGCCCACGAGTCCATCTTTC	-99,99 %
	HSP10	TGGTTGAAAGGAGTGCTGCT	TAGAACCCGATCCAACAGCG	-100 %
	P53	GATTTGATGCTGTCCCCGGA	CTGGCATTCTGGGAGCTTCA	241,76 %
Oxidative stress genes	GPX4	GCCTTCCCGTGTAACCAGTT	TTCATCCACTTCCACAGCGG	-76,94 %
	GPX1	TCCGGGACTACACCCAGATG	TCTTGGCGTTCTCCTGATGC	94,48 %
	GSR	ATGATCAGCACCAACTGCACG	TTAACCTCCTTGACCTGGGAGA	81,57 %
	CAT	AGCTTAGCGTTCATCCGTGT	GCCACTAGCTTGCATTTG	-38,19 %
	SOD1	TGCAGGTCCTCACTTTAATCCTC	AGTCTCCAACATGCCTCTCTTC	91,83 %
References genes	TBP	CACGAACCACGGCACTGATT	TTTTCTTGCTGCCAGTCTGGAC	-73,52 %
	GUSB	AGCCAGTTCCTCATCAATGG	GGTAGTGGCTGGTACGGAAA	-70,05 %
	GAPDH	TGTTCGTCATGGGTGTGAAC	ATGGCATGGACTGTGGTCAT	72,83 %
	SDHA	AGCAAGCTCTATGGAGACCT	TAATCGTACTCATCAATCCG	Undetermined
	RPS18	AGCTTGTTGTCCAGACCATT	TGAGGAAAGCAGACATTGAC	411,75 %
	ALAS1	ACACATCTTCCCCATGGCAG	TCCATAACTGCCCCACACAC	-37,15 %
	RPL9	CTCTGAAGGGACGCACAGTT	GTCAACCCGGAGCCTCTTTT	114,28 %
	ACTB	GAGCACAGAGCCTCGCCTTT	TCATCATCCATGGTGAGCTGG	76,53 %
	B2M	GATGAGTATGCCTGCCGTGT	CTGCTTACATGTCTCGATCCCA	103,25 %
	RPLP0	CGTCCTCGTGGAAGTGACAT	TAGTTGGACTTCCAGGTCGC	98,52 %
	UBC	CAGCCGGGATTTGGGTCG	CACGAAGATCTGCATTGTCAAGT	94,00 %

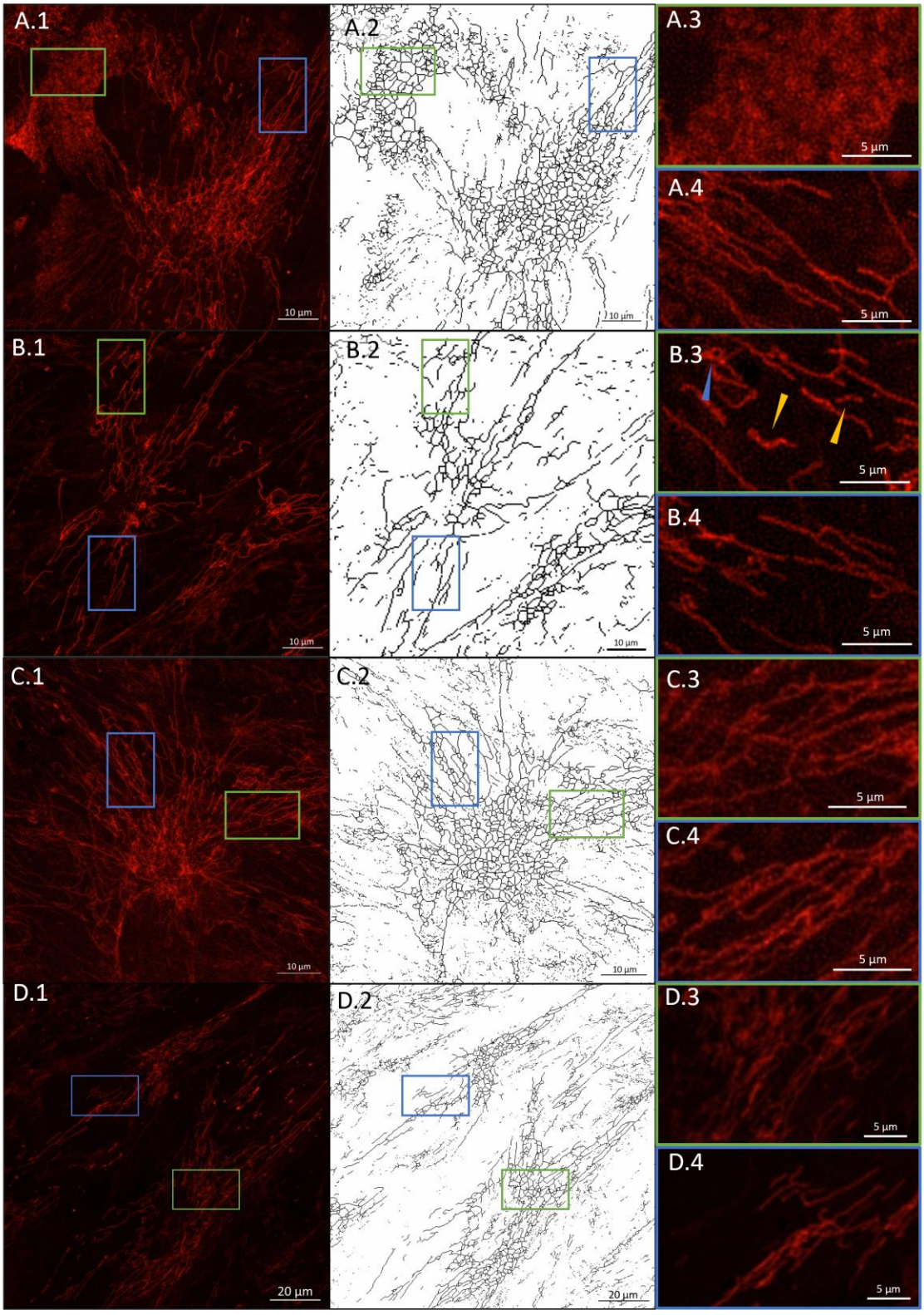

Figure S1 – Mitochondrial visualization with Mitotracker Red CMXRos after 7 days of NP exposure. Image A.1 - D.1 shows the overview picture. Image A.2 - D.2 are skeletonized images of A.1 – D.1. Images A.3 – D.3 and A.4 – D.4 3 are enlargement of the selected regions indicated with an green or blue border. **A**. Mitochondrial network of hDPSCs after 10 µg/ml PSNP exposure. **B**. hDPSCs mitochondria after 10 µg/ml AgNP exposure. Degradation of mitochondria complex was observed by the punctate morphology and smaller fragments. Blue arrow indicate swollen punctuate mitochondria, and yellow arrow indicate short mitochondria fragments. **C**. Visualization of mitochondria after exposure of 10 µg/ml TiO_2NPs to hDPSCs. **D**. hDPSCs mitochondria after 7 days of osteogenesis induction. Scale bars are present in the lower right corner of each figure. Images are taken with confocal microscopy with 40x water objective and laser 561 nm for MitoTracker Red CMXRos.

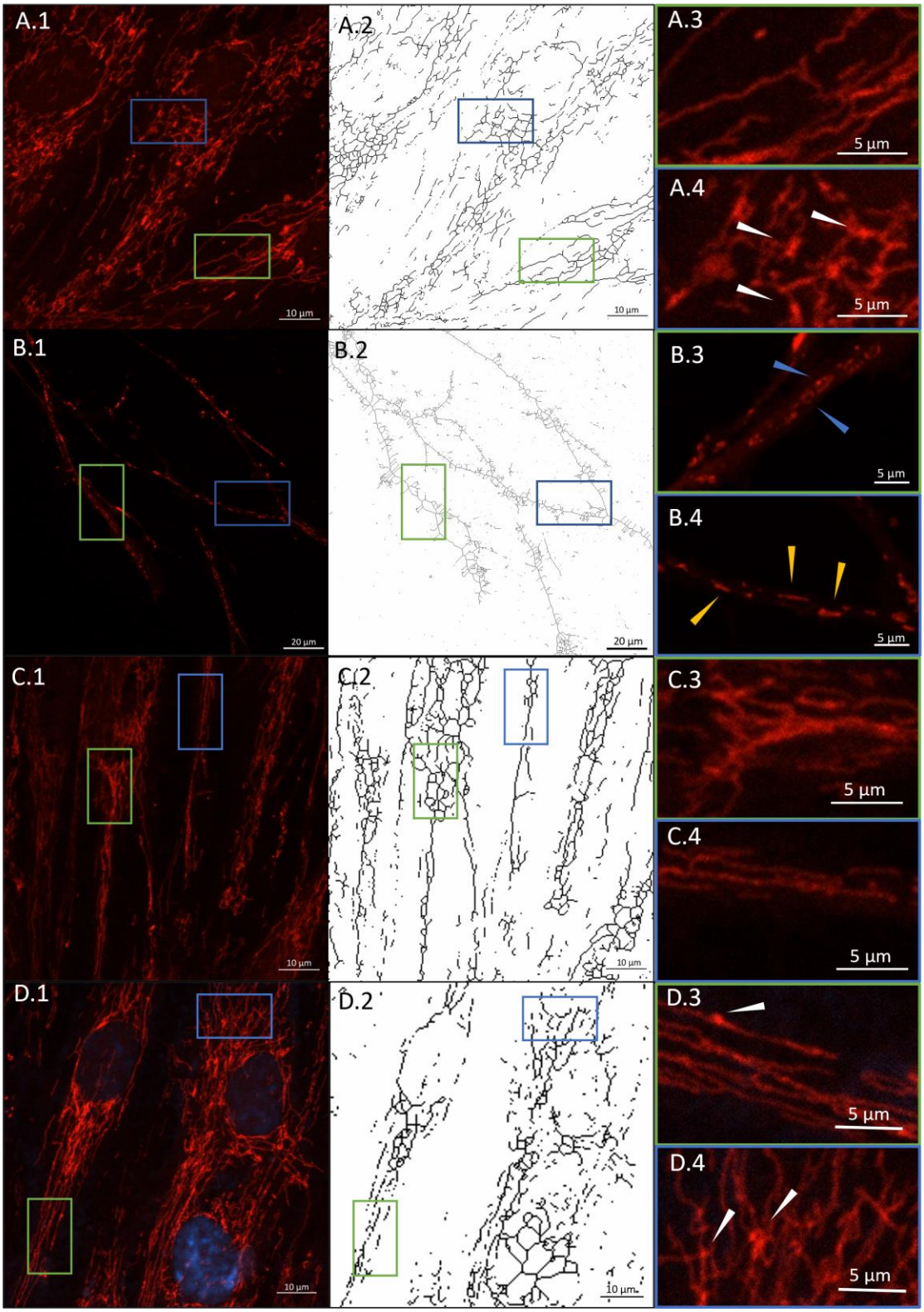

Figure S2 – Mitochondrial visualization with Mitotracker Red CMXRos after 3 days of NP exposure. Image A.1 - D.1 shows the overview picture. Image A.2 - D.2 are skeletonized images of A.1 – D.1. Images A.3 – D.3 and A.4 – D.4 3 are enlargement of the selected regions indicated with an green or blue border. **A**. Mitochondrial network of hDPSCs after 100 µg/ml PSNP exposure. White arrow indicate mitochondria thickening. **B**. hDPSCs mitochondria after 10 µg/ml AgNP exposure. Degradation of mitochondria complex was observed by the punctate morphology and smaller fragments. Blue arrow indicate swollen punctuate mitochondria, and yellow arrow indicate short mitochondria fragments. **C**. Visualization of mitochondria after exposure of 100 µg/ml TiO_2NPs to hDPSCs. **D**. hDPSCs mitochondria after 3 days of osteogenesis induction, white arrows indicate mitochondria thickning. Scale bars are present in the lower right corner of each figure. Images are taken with confocal microscopy with 40x water objective and laser 561 nm and 405 nm for MitoTracker Red CMXRos and Hoechst 33342 respectively.

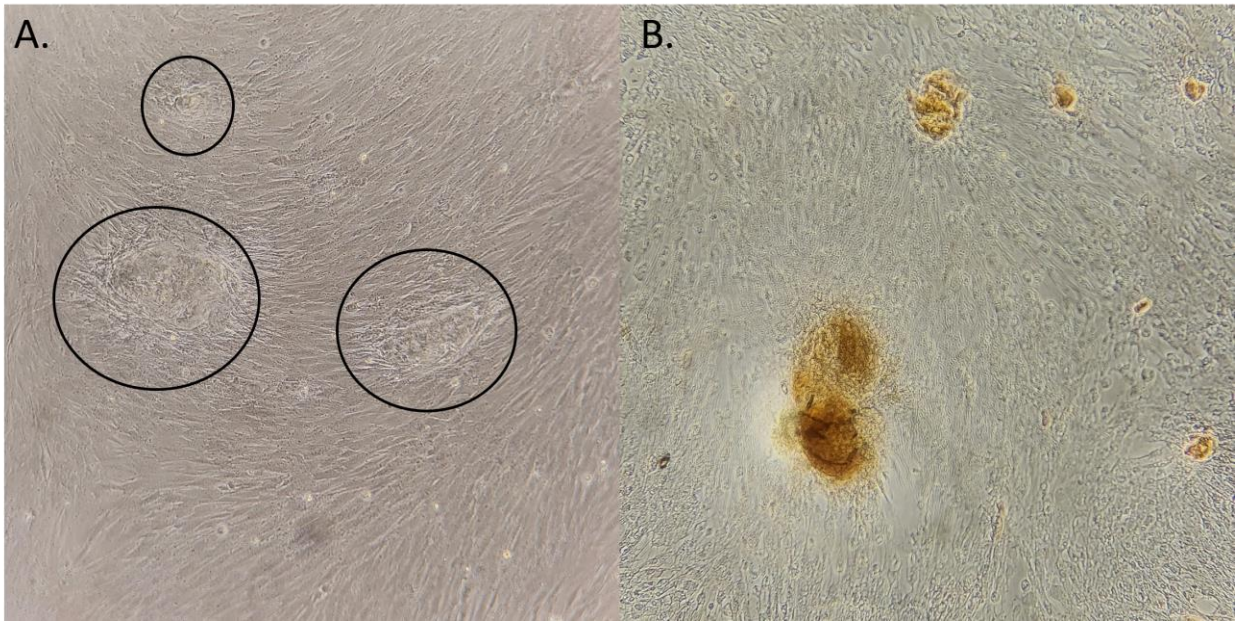

Figure S3 – Formation of differentiated cells in #10: A. Shows swollen structures that indicate of differentiated cells (encircled in black) after 3 days of osteogenesis induction. **B**. Shows stained calcium nodules with ARS staining, after 14 days of osteogenesis induction. Images are taken with inverted microscopy (Nikon DS-Fi3).